HHS Public Access

Author manuscript

J Comp Neurol. Author manuscript; available in PMC 2016 June 01.

Published in final edited form as:

J Comp Neurol. 2015 June 1; 523(8): 1258–1280. doi:10.1002/cne.23738.

Efferent innervation of turtle semicircular canal cristae: comparisons with bird and mouse

Paivi M. Jordan[1], **Margaret Fettis**[1], and **Joseph C. Holt**[1,2]

[1]Department of Otolaryngology; University of Rochester, Rochester, NY; USA

[2]Department of Neurobiology and Anatomy; University of Rochester, Rochester, NY; USA

Abstract

In the vestibular periphery of nearly every vertebrate, cholinergic vestibular efferent neurons give rise to numerous presynaptic varicosities that target hair cells and afferent processes in the sensory neuroepithelium. Although pharmacological studies have described the postsynaptic actions of vestibular efferent stimulation in several species, characterization of efferent innervation patterns and the relative distribution of efferent varicosities among hair cells and afferents are also integral to understanding how efferent synapses operate. Vestibular efferent markers, however, have not been well characterized in the turtle, one of the animal models utilized by our laboratory. Here, we sought to identify reliable efferent neuronal markers in the vestibular periphery of turtle, to utilize these markers to understand how efferent synapses are organized, and to compare efferent neuronal labeling patterns in turtle with two other amniotes using some of the same markers. Efferent fibers and varicosities were visualized in the semicircular canal of Red-Eared Turtles (*Trachemys scripta elegans*), Zebra Finches *(Taeniopygia guttata)*, and mice (*Mus musculus*) utilizing fluorescent immunohistochemistry with antibodies against choline acetyltransferase (ChAT). Vestibular hair cells and afferents were counterstained using antibodies to myosin VIIa and calretinin. In all species, ChAT labeled a population of small diameter fibers giving rise to numerous spherical varicosities abutting type II hair cells and afferent processes. That these ChAT-positive varicosities represent presynaptic release sites were demonstrated by colabeling with antibodies against the synaptic vesicle proteins synapsin I, SV2, or syntaxin and the neuropeptide calcitonin gene-related peptide (CGRP). Comparisons of efferent innervation patterns among the three species are discussed.

All correspondences should be sent to: Paivi M. Jordan, Ph.D., University of Rochester, 601 Elmwood Ave, Box 629, Rochester, NY 14642. Phone: 585-273-2780; Fax: 585-756-5334; Paivi_Jordan@urmc.rochester.edu.

CONFLICT OF INTEREST STATEMENT

For all authors on this manuscript, there were no real or perceived conflicts of interest that influenced this work.

ROLES OF AUTHORS

Each author had complete access to the full data set used in this study. All authors assume responsibility for the integrity and accuracy of the data and data analyses. Study concept and design: PMJ, JCH. Acquisition of data: PMJ, MF, JCH. Analysis and interpretation of data: PMJ, MF, JCH. Drafting of the manuscript: PMJ, JCH. Critical revision of the manuscript for important intellectual content: PMJ, JCH. Statistical analysis: PMJ, JCH. Obtained funding: JCH. Administrative, technical, and material support: PMJ. Study supervision: JCH.

Keywords

vestibular efferent; hair cell; vestibular afferent; turtle; bird; mouse; choline acetyltransferase; synapsin; SV2; calretinin; AB_90764; AB_2068506; AB_2079751; AB_2314177; AB_10015251; AB_2282417; AB_2200400; AB_2315408; AB_477483; SciEx_12080

INTRODUCTION

The vestibular organs of nearly every vertebrate are endowed with a prominent cholinergic efferent innervation that originates bilaterally from e-group nuclei within the dorsal brainstem and then courses through cranial nerve VIII to innervate the vestibular periphery (Lysakowski and Goldberg, 2004; Meredith, 1988; Fayyazuddin et al., 1991). Within each end organ, electron microscopy (EM) studies have demonstrated that vestibular efferent neurons give rise to numerous bouton varicosities that synapse on type II hair cells, on bouton afferents innervating type II hair cells, as well as the terminal processes of calyx and dimorphic afferents when type I hair cells are present as seen in reptiles, birds, and mammals (Sans and Highstein, 1984; Lysakowski, 1996; Lysakowski and Goldberg, 1997; Holt et al., 2006; Li et al., 2007; Castellano-Muñoz et al., 2010). Vestibular efferent endings on type I hair cells, however, are infrequent. Vestibular efferent varicosities contain hundreds of small, clear vesicles (per μm^2) that often accumulate along sides of apposition with postsynaptic targets, demarcated by subsynaptic cisterns in hair cells and synaptic densities on afferent processes (Holstein et al., 2004; Holt et al., 2006; Li et al., 2007; Castellano-Muñoz et al., 2010). Immunohistochemical detection of choline acetyltransferase (ChAT), the rate-limiting enzyme in ACh synthesis, has confirmed that these heavily-vesiculated efferent varicosities are cholinergic (Kong et al., 1994b, 1998; Ohno et al., 1993).

Although a functional role for vestibular efferents has not been established, the deposition of cholinergic efferent varicosities along the interface between hair cells and primary afferents underscores their likely importance in vestibular processing. Not surprisingly given their innervation patterns, electrical stimulation of vestibular efferent neurons dramatically modifies the background discharge of vestibular afferents. In fish and mammals, efferent activation excites vestibular afferents (Highstein and Baker, 1985; Goldberg and Fernandez, 1980) while in bird, frog and turtle, efferent stimulation results in afferent inhibition and/or excitation (Rossi et al., 1980; Dickman and Correia, 1993; Brichta and Goldberg, 2000b). Much of our understanding about the synaptic mechanisms underlying these diverse vestibular afferent responses to efferent stimulation has come from pharmacological studies in frog and turtle. In line with ChAT expression in vestibular efferent neurons, the release of acetylcholine (ACh) and subsequent activation of ACh receptors on hair cells and afferents, at least in frog and turtle, account for many of these inhibitory and excitatory responses (Rossi et al., 1980; Bernard et al., 1985; Sugai et al., 1991; Holt et al., 2006). Efferent synaptic mechanisms in birds and mammals, on the other hand, have not been fully characterized, but similarities in the organization of hair cells, afferent innervation, and efferent synaptic structure suggest that efferent studies in the turtle might be directly

applicable to these other species (Brichta and Peterson, 1994; Lysakowski, 1996; Lysakowski and Goldberg, 1997; Brichta and Goldberg, 2000a, 2000b; Jordan et al., 2013).

In the turtle crista, afferent responses to efferent stimulation vary considerably depending on afferent class (e.g. bouton versus calyx) as well as an afferent's location in the neuroepithelium (Brichta and Goldberg, 2000b; Holt et al., 2006). For example, bouton afferents near the non-sensory torus are profoundly inhibited during efferent stimulation while bouton afferents near the planum are weakly excited. In contrast, calyx-bearing afferents, restricted to the central zone, are profoundly excited by efferent stimulation. In turtle, the variation in afferent responses to efferent stimulation has been attributed to the activation of distinct nicotinic and muscarinic ACh receptors on hair cells and afferents (Holt et al., 2006; Jordan et al., 2013). In addition to diversity in postsynaptic receptor mechanisms, we hypothesized that morphological differences in efferent innervation might also contribute to response variability in turtle.

While EM data has provided unparalleled detail in identifying efferent synapses on hair cells and afferents (Holt et al., 2006), it has not allowed for a more global view of the general efferent innervation patterns across the turtle crista. An alternative approach, where such a view is possible, has relied on light microscopy and immunohistochemical detection of ChAT (Kong et al., 1994b; Popper et al., 2002; Jordan et al., 2013; Pujol et al., 2014). But specifying which ChAT-positive processes are synaptic would be further strengthened by additional labeling with distinct pre- and postsynaptic markers, as has been demonstrated at efferent (Zidanic, 2002; Osman et al., 2008; Wibowo et al., 2009; Roux et al., 2011) and afferent synapses in the auditory system (Khimich et al., 2005; Liberman et al., 2011). Several studies have investigated the distribution of efferent presynaptic or postsynaptic proteins in the peripheral vestibular system (Favre et al., 1986; Tanaka et al., 1989; Ishiyama et al., 1995; Dailey et al., 2000; Holstein et al., 2005; Luebke et al., 2005, Osman et al., 2008; Castellano-Muñoz et al., 2010), but seldom in the context of co-labeling with ChAT (Luebke et al., 2014). We addressed this gap using fluorescent immunohistochemistry with antibodies to ChAT and several well-characterized presynaptic markers to label cholinergic vestibular efferent fibers and varicosities in the crista of turtle (*Trachemys scripta elegans)*, zebra finch (*Taeniopygia guttata*), and mouse (*Mus musculus*).

MATERIALS AND METHODS

Tissue acquisition and fixation

For this study, vestibular tissues were acquired from 50 Red-Eared Turtles (*Trachemys scripta elegans*), 10 Zebra Finches (*Taeniopygia guttata*), and 10 mice (*Mus musculus*). Both sexes of turtles, 100–400 g (7–14 cm carapace length) were purchased from Kons Direct (Germantown, WI) or Cyr's Biology Supply (Pontchatoula, LA). Adult Zebra Finches of both sexes were obtained commercially from Magnolia Bird Farm (Anaheim, CA) or raised in an aviary in the Department of Brain and Cognitive Sciences at the University of Rochester. Adult female C57BL/6 mice (strain code 027), > 6 weeks old, were obtained from Charles River Laboratories (Wilmington, MA). All animal procedures were in accordance with recommendation made by NIH's Guide for the Care and Use of Laboratory

Animals and approved by the University Committee on Animal Resources (UCAR) at the University of Rochester.

Turtles were decapitated following pentobarbital overdose, and the head was bisected along the sagittal plane and placed in an oxygenated turtles Ringer's solution containing (in mM): 105 NaCl, 4 KCl, 0.8 $MgCl_2$, 2 $CaCl_2$, 25 $NaHCO_3$, 2 Na-pyruvate, 10 glucose, 0.5 glutamine (all from Sigma, St. Louis, MO), pH 7.2–7.3 after bubbling with 95% O_2/5% CO_2. The entire membranous labyrinth was dissected and freed from the surrounding bone and subsequently placed into freshly prepared, 4% paraformaldehyde (PFA) in phosphate buffer (0.1M PB, pH 7.4) for 2–12h at 4°C. Adult Zebra Finches were decapitated as previously described (Tremere et al., 2009). After quick removal of brain for an unrelated study, both temporal bones were extracted and a small cut was made through the bony and membranous posterior canal to permit tissue access before dropping into 4% PFA for 4–12h at 4°C. Mice were anesthetized with ketamine/xylazine (100mg and 10mg/kg, respectively) followed by transcardial perfusion with phosphate-buffered saline (PBS, 0.9% NaCl in 0.1 M PB) and freshly prepared 4% (w/v) PFA. Temporal bones were removed and post-fixed in 4% PFA for 4–12h at 4°C. Following fixation in PFA, the membranous labyrinth of bird and mouse were carefully extracted from the temporal bone and transferred to 0.1M PB.

Preparation and sectioning of vestibular end organs

Fixed, microdissected vestibular tissues were washed repeatedly (>30 mins) in 0.1M PB. Segments of membranous labyrinth opposing the neuroepithelium were excised allowing unobstructed access to the apical surface of the tissue. Although we were primarily interested in semicircular canal cristae, in a few instances, we also examined otolithic maculae. For turtle whole organ staining, vestibular tissue was transferred to a collection chamber for blocking and further immunohistochemical processing. For sections, vestibular tissue was first placed in a 30% sucrose/0.1M PB solution at 4°C for 1–12 hours and then embedded in 12% gelatin (Difco; Becton and Dickinson, Sparks, MD) prepared in 30% sucrose. Neuroepithelia were sectioned at 40 μm (either longitudinally or transversely, see Fig. 1B) on a freezing microtome (American Optical), and the resulting sections were transferred to a glass collection chamber filled with 0.1M PB. The collection chamber was fitted at one end with a fine wire mesh and stopcock to allow repeated washes while retaining tissue sections. The collection chamber was warmed to de-gelatinize the tissue sections and melted gelatin was then removed by draining the chamber. Remaining tissue sections were washed several times in 0.1M PB prior to the start of the IHC process.

Immunohistochemical procedures

Standard immunohistochemical procedures were used to label select proteins in whole organ crista preparations as well as vestibular tissue sections. Washes, blocking, and incubation with primary and secondary antibodies were carried out in tissue collection chambers at room temperature under gentle agitation on the stage of an orbital shaker. Blocking solution, composed of 5% normal goat serum (NGS, Jackson Immunoresearch; West Grove, PA) and 0.5% Triton X-100 in 0.1M PB (all from Sigma; St. Louis, MO), was added for 1h. Block was removed and primary antibodies diluted in 0.1M PB were allowed to react overnight. Table 1 summarizes the immunogen, source, specificity controls, and working dilutions of

primary antibodies utilized in this study. The following day, primary antibodies were removed and sections were gently washed 5X @ 5 mins each with 0.1M PB prior to the addition of Alexa-Fluor® 488, 594, or 647-conjugated secondary antibodies (Invitrogen, Carlsbad CA) diluted at 1:200–500 in 0.1M PB. Sections were incubated in secondary antibodies for 2–3h in the dark followed by washing with PB (5X @ 5mins each). After washing, DAPI (4′,6′-diamidino-2-phenylindole, Sigma, St. Louis, MO) was prepared at a concentration of 1μg/ml in distilled water and added to the collection chamber for 5 min to counterstain cell nuclei. Sections were subsequently followed by one additional wash in distilled water, transferred to a Sylgard dish, and then moved onto Superfrost Plus® slides (VWR; West Chester, PA) using an eyelash probe. After drying, sections were cover-slipped using Vectashield® (Vector Laboratories; Burlingame, CA) or SlowFade Gold mounting medium (Invitrogen, Carlsbad, CA) and sealed with clear nail polish. Slides were stored in the dark at 4°C until imaging.

Antibody Characterization

The ChAT AB144P antibody (Millipore Cat# AB144P RRID: AB_2079751) utilized in this study was generated in goat against the whole enzyme isolated from human placenta that is identical to the brain enzyme (Bruce, 1985). Within the auditory and vestibular system, AB144P has been characterized in the inner ear of lizard (Wibowo et al., 2009), mouse (Kong et al., 2002), rat (Kong et al., 1994b) and human (Kong et al., 1994a, 1998). This ChAT antibody has been shown by western blot to detect a single 68–70kd band in turtle retina, as well as the brains of fish, lizards, and rat (Anadón et al., 2000; Lee et al., 2007; Wibowo et al. 2009). In our hands, we detected a doublet of bands via western blotting at ~70kd in turtle or a single band with mouse brain tissue extracts running at a slightly higher MW (Fig. 1). Another polyclonal ChAT antibody (RRID: AB_2314177) was generated in rabbit against immunopurifed chicken ChAT (Johnson and Epstein, 1986) and validated in western blots and immunohistochemistry with chick spinal cord using preadsorption controls. This ChAT antibody is also noted for staining inner ear efferents (Zidanic 2002).

The anti-synapsin antibody utilized in this study (Millipore Cat# AB1543 RRID: AB_2200400) detects synapsin Ia and Ib and was derived from synapsin I extracts purified from bovine brain. Synapsin antibodies have been used to demarcate efferent varicosities in rat, mouse, and guinea pig cochlea (Layton et al., 2005; Bergeron et al., 2005; Lopez et al., 2008), the vestibular labyrinth of toadfish (Holstein et al., 2005) as well as frog saccule (Castellano-Muñoz et al., 2010).

The anti-SV2 monoclonal antibody (DSHB Cat# SV2 RRID: AB_2315408) developed by K. Buckley was obtained from the Developmental Studies Hybridoma Bank developed under the auspices of the NIDCHD and maintained by the Univ. of Iowa, Dept. of Biology, Iowa City, IA 52242. This antibody has previously been well characterized and shown to label synaptic vesicles in several vertebrate species including lizard (Wibowo et al., 2009), owl (Kubke et al., 2002), guinea pig (Layton et al., 2005), and rat (Mandell et al., 1990; Brooke et al., 2010). Furthermore, western blotting with this antibody recognizes a distinct protein band (~70–90kd) in a wide variety of species including chicken, rabbit, mouse, and

bovine brain extracts and specifically in rat retina and lizard basilar papilla (Buckley and Kelly, 1985; Mandell et al., 1990; Wibowo et al., 2009).

The syntaxin antibody utilized in this study (Sigma-Aldrich Cat# S0664 RRID: AB_477483) was generated against the synaptosomal plasma membrane fraction from adult rat hippocampus. In western blots, this antibody labels a single band of 35kd MW in rat and fish (Barnstable et al., 1985; Inoue et al. 1992; Ramakrishnan et al., 2006). It has been used for immunolabeling in a variety of tissues and has reported reactivity against rabbit, rat, bovine, and trout tissues (Hennig and Cotanche, 1998; Ramakrishnan et al., 2006; see also manufacturer's data sheet). In the ear, syntaxin has been localized within the SNARE complex of proteins necessary for transmitter release in both inner and outer hair cells in rat and guinea pig organ of corti (Safieddine and Wenthold, 1999) and has been localized to efferent endings on hair cells in chick and trout (Hennig and Cotanche, 1998; Ramakrishnan et al., 2006).

The myosin VIIa antibodies utilized for this study have been well characterized by others and shown to specifically label hair cells in mouse, rat, rabbit and frog cochlear tissue. The polyclonal myosin VIIa antibody (Proteus Biosciences Cat# 25-6790 RRID: AB_10015251) was generated in rabbits immunized with a peptide corresponding to amino acids 880–1077 from the tail region of human myosin VIIa. In particular, immunohistochemistry with this antibody was used to successfully label type I and type II hair cells in guinea pig (Hasson et al., 1995), mouse (Boëda et al., 2001; Pujol) and bird (Duncan et al., 2006) cochlea and demarcated a single band of ~220kDa in western blots of rat ear tissues (Hasson et al., 1995). The monoclonal myosin VIIa (DSHB Cat# MYO7A 138-1 RRID: AB_2282417) antibody was generated by Dana Jo Orten and was obtained from the Developmental Studies Hybridoma Bank developed under the auspices of the NICHD and maintained by the Univ. of Iowa, Dept. of Biology, Iowa City, IA 52242. This antibody was prepared against amino acids 927–1203 of the human myosin VIIa transcript 2 and expressed in E. coli. It has been shown to react against human, mouse, rat and chicken tissues (DSHB). Soni et al. (2005) further characterized this antibody and successfully showed it labeled rat retinal cells in the expected pattern. Additionally, experiments in our lab showed identical hair cell labeling between this monoclonal and the Proteus polyclonal myosin VIIa antibodies. For this study, both myosin VIIa antibodies were utilized depending upon the species used for double labeling experiments (e.g. tissues labeled with polyclonal synapsin I were double labeled with the monoclonal myosin VIIa while monoclonal SV2 stained tissues were double labeled using the polyclonal myosin VIIa).

Our calretinin antibodies (RRID: AB_90764, RRID: AB_2068506) are goat and rabbit polyclonal antibodies generated to recombinant rat calretinin. These antibodies recognize a 28–30 kDa band in turtle cochlear tissues (Hackney et al. 2003) and mouse brain (Liu and Davis, 2014). Calretinin antibodies label calyx only afferents in the vestibular end organs of gerbils, rats, mice, and other rodents (Desai et al., 2005a,b; Leonard and Kevetter, 2002) as well as some type II vestibular hair cells in the utricular macula and canal crista (Desai et al., 2005a,b). In turtle neuroepithelia, calretinin labels both vestibular afferents and hair cells (Monk and Peterson, 1995; Huwe et al., 2011).

Two CGRP antibodies, (MU33 and JH84; rabbit polyclonals) were generously provided by Ian M. Dickerson. MU33 was generated against the amidated carboxyl 7 amino acids of rat αCGRP while JH84 was generated against mature rat αCGRP (Rosenblatt and Dickerson, 1997). Antibody specificity was validated using immunoprecipitation (Rosenblatt and Dickerson, 1997). These antibodies label cholinergic efferent neurons in the guinea pig cochlea and mouse semicircular canal cristae (Cabanillas and Luebke, 2002; Luebke et al. 2014).

Imaging and post-imaging analysis

Images were first acquired with a Zeiss Axio Imager motorized upright multifluorescent microscope outfitted with an Apotome slider system (Zeiss Imaging Systems, Oberkochen, Germany) for acquisition of z stacks. Images were post-processed using Axiovision (Zeiss Imaging Systems, Oberkochen, Germany) and/or Adobe Photoshop CS6 (Adobe Systems, San Jose, CA) software to adjust contrast and brightness within the linear range. Selected tissue slides were also imaged in the URSMD Confocal and Conventional Microscopy Core (RRID: SciEx_12080) using an Olympus FV1000 Laser Scanning Confocal microscope (Olympus America, Center Valley, PA) with a 20x UPlanS-Apo (NA 0.85), 60x (NA1.42), or 100x Plan-Apo (NA 1.4) oil objective, with Kalman setting (i.e. line averaging) of 0–3, and sequential scanning option. The confocal aperture (pinhole) was fixed at 1 Airy unit for all objectives and fluorophores using the auto settings in the Olympus FV1000 acquisition software. For each objective, optimized Z-slice thickness was determined based on the Nyquist formula, also using auto settings in the acquisition software. Confocal images were processed using Olympus FV1000 software and adjusted in the linear range to improve contrast and/or brightness. Final figures were cropped in Photoshop and imported into Adobe Illustrator for labeling and creating figure panels.

Automatic Counts and Measurements of ChAT-positive varicosities

Turtle cristae were immunostained for ChAT and imaged as described above using the confocal microscope outfitted with a 60x Plan-Apo oil immersion lens with a z thickness of 0.42μm. Automatic counts of ChaT-positive varicosities were performed as follows: Hemicristas were split into three regions, each approximately 150μm in length and designated planum, central and torus. Within a single z plane in each zone, 5–6, 20μm × 20μm (i.e. 400μm^2) boxes were drawn across the synaptic region where the number and area of ChAT-positive varicosities per box were automatically tabulated using Image Pro Plus (7.0) (Media Cybernetics, Rockville, MD). Briefly, for the automated counting and area determination, single z plane images were exported as raw data sets from Olympus FV1000 software and opened in Image Pro where the correct scaling was chosen. Using the Count/Size setting and manually thresholding each image to a setting of ~50–255 gray scales allowed for the best representation of ChAT-positive varicosities. Occasionally, the software could not automatically determine between adjacent varicosities in which case varicosities were separated using the edit manual split feature. The number of varicosities per 20μm × 20μm box as well as the area of each varicosity were compiled in Microsoft Excel and then imported into GraphPad Prism (GraphPad Software, LaJolla, CA) for graphing and statistical analyses. At least three separate experiments from six animals were used to

acquire these data. Manual counts by an unbiased observer were also done on a select set of images to confirm the automatic count data.

Colocalization analysis

Confocal z stacks of turtle crista sections, stained for either ChAT, synapsin I (SynI), and SV2 or ChAT and CGRP, were acquired with either the 60X or 100X objectives. A total of 3 separate immunohistochemical experiments (i.e. 3 animals) were utilized for each set. In individual z planes from each stack (n=4 for ChAT, SynI and SV2; n=3 for ChAT and CGRP), ROI's were drawn around 10–20 individual ChAT-positive puncta. In order to minimize selection bias, channels used to stain SynI, SV2, or CGRP were turned off during ROI designation. A total of 57 puncta were analyzed for ChAT, SynI, and SV2 while 52 puncta were used for ChAT and CGRP. A Pearson colocalization coefficient (PCC; Manders et al., 1992) was determined for each punctum using the colocalization function in the Olympus FV1000 software. The PCC is a measure of the covariance in the gray values of fluorescence intensity between two signals (i.e. ChAT vs. SynI or ChAT vs. CGRP) on a pixel-by-pixel basis. A scatter plot was generated for each ChAT-positive punctum by plotting the corresponding gray scale intensity values of each fluorophore for each and every pixel within the ROI. The slope from the linear fit of this data provided the PCC that theoretically ranges from −1 to +1 with a coefficient of −1 indicating an inverse correlation between the gray values (fluorescence intensity) of the two channels, 0 indicating no colocalization, and +1 indicating perfect colocalization of the two fluorophores (Manders et al., 1992). Colocalization data were imported into Graph-Pad Prism (La Jolla, CA) for graphing and statistical analyses (see Statistical procedures below). Reported PCC values reflect the mean PCC ± SEM for the population of sampled varicosities.

Estimation of efferent and afferent fiber diameters

To calculate the approximate fiber diameter of calretinin and ChAT-positive fibers, ten single calretinin-positive and ten single ChAT-positive fibers for each species studied were measured using Axiovision (Zeiss Imaging Systems, Oberkochen, Germany) software. Since some images may not have encompassed the entire fiber diameter, measurements were taken from the widest point visible on 5–10 μm thick z stacked images, at a distance of 40μm or less from the hair cell layer. Fiber diameter data were imported into Graph-Pad Prism (La Jolla, CA) for graphing and statistical analysis (see Statistical procedures below).

Statistical procedures

All statistical analyses were done in Graph Pad-Prism (GraphPad Software, La Jolla, CA). Unless otherwise stated, values are expressed as means ± SEM. A one-way ANOVA with Bonferroni post hoc comparisons was used to evaluate if varicosity counts and areas differed among regional zones of the turtle crista neuroepithelium. One-sample t-tests were used to evaluate if mean PCC values differed from zero (McDonald and Dunn, 2012). A two-way ANOVA and Bonferroni planned comparison post hoc tests (Graph Pad-Prism; La Jolla, CA) were used to compare afferent and efferent fiber diameter across turtle, zebra finch, and mouse.

Western blotting

Turtle brain, mouse brain, and turtle inner ear tissue (5 ears, 3 animals) were separately lysed using RIPA buffer (Fisher Scientific) with 1 mM each of phenylmethylsulfonyl fluoride (PMSF) and protease inhibitor cocktail (Sigma, St. Louis, MO). Samples were homogenized on ice for 30s, allowed to settle overnight at 4°C, and then centrifuged at 20,000g for 10 min also at 4°C. Supernatant was removed and inner ear tissue was concentrated using a centrifugal filter unit (Amicon, Fisher Scientific, Waltham, MA). All samples were quantified by using a BCA protein quantification kit (Pierce, Rockford, IL). Twenty micrograms of total protein were diluted in Nu-PAGE LDS sample buffer and NuPAGE reducing agent (both from Invitrogen, Carlsbad, CA) and heated to 70°C for 10 min. Negative controls substituted diH20 for protein extract. Samples were then briefly vortexed, centrifuged, and loaded onto 4–12% NuPAGE Novex Bis Tris Gels and electrophoresed at room temperature at 150 V for 2 hr. Gels were transferred onto Hybond ECL nitrocellulose membrane (Amersham Biosciences U.K.) by electrophoretic transfer at 30 V for 1 hr. Membranes were blocked with 5% normal serum in 0.1%TBS-Tween for 1hr followed by 1–2 rinses (5 mins each) with 0.1% TBS-T and immunoblotting with ChAT (1:1000 in 0.1%-TBS-T) overnight at 4°C. Membranes were then washed six times, for 10 min each, with 0.1% TBS-Tween and incubated for 1 hr at room temperature with the appropriate horseradish peroxidase conjugated secondary antibody (Amersham Biosciences U.K.). Membranes were again washed six times, for 10 min each, and immunoreactive bands were detected by using a chemiluminescent Western blot detection kit (Amersham Biosciences U.K.). Blots were exposed to ECL hyperfilm (Amersham Biosciences, UK) for 30s to 5 min prior to developing.

RESULTS

ChAT immunohistochemistry in the turtle crista

Vestibular efferent neurons are predominantly cholinergic and as such should express the cholinergic marker choline acetyltransferase (ChAT). Although ChAT immunohistochemistry has been often used to label efferents innervating the inner ear in a number of vertebrate species (Kong et al., 1994a, 1994b, 2002; Wibowo et al, 2009), comparable data in turtle has been lacking. Therefore, we sought to determine if ChAT labeling would be helpful in identifying efferent neurons in turtle semicircular canal cristae. For this task, we utilized goat antibodies directed against the whole ChAT enzyme isolated from human placenta that is identical to the brain enzyme (Bruce, 1985). First, to verify the specificity of the ChAT antibody, we probed a series of western blots from turtle brain and turtle ear. We also included mouse brain as an additional control. The ChAT antibody used in this study has been shown previously to detect a single 68–70kd band in turtle retina (Lee et al., 2007). In agreement with that study, we detected a prominent band of the appropriate size (~73kDa) in both turtle brain and ear (Fig. 1A). We also detected a much fainter second band at ~68kDa. Multiple bands may be indicative of posttranslational modification, degradation products, or multiple isoforms (Oda, 1999; Anadón et al., 2000). In mouse brain extracts, we only detected a single band running at a slightly higher MW of ~75kDa.

Since the organization of vestibular hair cells and afferents has been described for the turtle semicircular canal crista (Brichta and Peterson, 1994; Brichta and Goldberg, 2000a), we focused our initial efforts on labeling efferent neurons in the crista neuroepithelium (Fig. 1B–D). Turtle posterior and anterior cristae consist of two saddle-shaped hemicristae whereas the horizontal canal is comprised of a single hemicrista. Each crista contains both type I and type II hair cells. Type I hair cells are restricted to the central zone (CZ) whereas type II hair cells are distributed throughout the neuroepithelium including the CZ and peripheral zone (PZ) (Fig. 1B). A whole mount preparation of the turtle posterior crista was immunostained for ChAT and the hair cell marker, Myosin VIIA (Myo7A) (Fig. 1C). Consistent with hair cell staining, Myo7A labeling was restricted to the neuroepithelium where it outlined the boundaries of each hemicrista. In longitudinal crista sections, we identified that Myo7A staining, in fact, was confined to the hair cell layer (Fig. 1D). Antibodies to ChAT labeled a dense neural network that appeared to populate the entire crista neuroepithelium (Fig. 1C, 1D). This can be better appreciated with ChAT staining in the longitudinal sections where over a 100 small-diameter (~1 μm), ChAT-positive fibers are seen coursing through the stroma (Fig. 1D). Although individual ChAT-positive fibers can be identified (arrowheads), they often traveled together in discrete bundles of 3 or more fibers. The density of ChAT-positive fibers across the stroma was generally correlated with the width of the neuroepithelium, gradually increasing as one moves from the narrow torus region towards the wider planum regions (Fig. 1D, right side). Efferent fibers were routinely missing from a small band centered on the non-sensory torus region (*, Fig. 1D). Upon reaching the supporting cell layer, demarcated by dense DAPI staining, ChAT-positive fibers underwent an extensive amount of branching to give rise to many spherical puncta concentrated along the base of the hair cell layer (Fig. 1D). Comparable ChAT staining was seen in all three turtle canal cristae as well as the utricular macula (data not shown). Similar immunostaining patterns were seen with antibodies generated against ChAT derived from chick brain (data not shown; Johnson and Epstein, 1986). Collectively, these data suggested that antibodies to ChAT were labeling vestibular efferent neurons in the turtle crista.

Across the vertebrate scale, type II hair cells are a common synaptic target for vestibular efferent neurons (Fig. 2A). The dense deposition of ChAT-positive puncta within the hair cell layer of the turtle crista should certainly place efferent neurons in close apposition with type II hair cells. For closer inspection, we sampled stretches of neuroepithelium adjacent to the torus and planum, two regions of the crista where only type II hair cells reside (Fig. 2B inset). In both regions, much of the cytoplasm of type II hair cells was immunostained for Myo7A with the exception of the space occupied by the nucleus (Fig. 1D, 2D, 2E). Bundles of ChAT-positive fibers traversed the stroma and gave rise to many smaller fibers that were frequently interrupted by spherical or ovoid varicosities (Fig. 2C). The majority of these varicosities occupied the basal pole of type II hair cells in regions beneath or adjacent to hair cell nuclei (Fig. 2D). Occasionally, ChAT-positive varicosities were also identified along the apical half of the hair cell layer (Fig. 2D, arrowheads) as well as within lower reaches of the supporting cell layer (Fig. 2D, arrows). ChAT-positive varicosities, however, were absent from deeper portions of the stroma. Examination of type II hair cells in the PZ near the planum revealed similar ChAT staining as seen in the torus (Fig. 2E). Orthogonal views

confirmed that ChAT-positive varicosities were directly adjacent to type II hair cells (Fig. 2E1, E2). Most type II hair cells received two to five such varicosities.

Calretinin labeling of hair cells and afferents in turtle

In addition to innervating type II hair cells, efferent neurons innervate the terminal processes of afferent fibers including bouton afferents in fish (Sans and Hightein, 1984) and both bouton and calyx-bearing afferents in turtle, bird, and mammals (Holt et al., 2006; Li et al., 2007; Lysakowski and Goldberg, 1997, 2008) (See Fig. 3A). We reasoned that ChAT-positive varicosities seen well below the hair cell layer might in fact be innervating afferent processes. In order to ascertain if these ChAT-positive varicosities were in close apposition to afferent processes, we required an afferent marker. To label afferent fibers in the turtle crista, we then decided to use antibodies directed against the calcium-binding protein calretinin. Calretinin expression has traditionally been used to label calyx only afferents in the vestibular end organs of gerbils, mice, and other rodents (Desai et al., 2005a,b; Leonard and Kevetter, 2002). It should be noted, however, that calretinin also labels some type II vestibular hair cells in the utricular macula as well as the crista (Desai et al., 2005a,b). In turtle neuroepithelia, previous data indicated that calretinin is expressed by both vestibular afferents and hair cells (Monk and Peterson, 1995; Huwe et al., 2011).

Calretinin immunolabeling in the turtle crista demonstrated three major patterns of staining: (1) Calretinin clearly stained calyx-bearing afferents across the central zone including calyx and dimorphic afferents (Fig. 3B, arrowhead and asterisk, respectively). Here, calretinin immunohistochemistry labeled the full length of these afferents, from deep within the stroma to the apical calyceal endings near the top of the neuroepithelium; (2) Bouton afferents in the peripheral zone near the torus were also routinely stained by antibodies to calretinin (Fig. 3B, arrow). The label was limited to several bouton afferents bordering the central zone but absent from bouton afferents closer to the torus; and, (3) We observed strong calretinin labeling of type II hair cells in the peripheral zone near the planum (Fig. 3B, see also Fig. 2E). Calretinin immunoreactivity was noticeably absent from supporting cells, type I hair cells and type II hair cells near the torus.

In order to visualize how efferent varicosities were localized with respect to afferent processes, we performed immunolabeling experiments for ChAT and calretinin (Fig. 3C–E). In transverse sections through the central zone, many ChAT-positive varicosities were positioned clearly below the hair cell layer where they often aggregated along the first 10–20 μm of the axonal stalk, just below the calyceal expansion (Fig. 3C). Proximity to the parent fiber was confirmed in orthogonal views (inset, Fig. 3C). In the example shown, four to five varicosities were clustered around the axon. ChAT-positive varicosities were also found abutting calyceal endings enclosing type I hair cells (arrows, Fig. 3C). ChAT-positive varicosities were similarly distributed along dimorphic afferents (Fig. 3D). ChAT-positive varicosities were also scattered along the terminal processes of calretinin-positive bouton afferents near the torus (Fig. 3E). ChAT-positive varicosities were often adjacent to bouton afferent terminals but it was difficult to reconcile if this represented direct contacts or simply a convergence of efferent and afferent synapses upon the base of type II hair cells. However, direct contacts could often be identified where ChAT-positive varicosities populated bouton

afferents prior to branching (arrowheads, Fig. 3E). An orthogonal view indicates their proximity to the parent fiber (inset, Fig. 3E).

Zonal variations among ChAT-positive varicosities in turtle

We next wanted to determine if the number of ChAT-positive varicosities varied with respect to region. Counts of ChAT-positive varicosities were performed for each of the zones across the turtle crista (i.e. planum, central and torus). In the planum region, 6.67 ± 0.48 ChAT-positive varicosities per 400μm ^{2} area were identified, while in the central zone there were 8.28 ± 0.47 and in the torus region 9.44 ± 0.87 ChAT-positive varicosities per 400μm ^{2} area (n=18 for each region; Fig. 3F). ChAT-positive varicosity counts from planum and torus regions were significantly different ($p<0.01$; one way ANOVA with Bonferroni post hoc analysis) while the central region was not significantly different from either the torus or planum regions. ChAT punctal area was also measured from confocal images. The average punctal area was 3.27 ± 0.17 μm^2, 3.34 ± 0.17 μm^2, and 3.39± 0.17 μm^2 for torus, planum and central regions, respectively (Fig. 3G). Punctal areas were not significantly different from one another ($p=0.87$). (All data presented as mean ± SEM).

Colocalization of ChAT, SYN I and SV2 in Turtle Efferent Varicosities

If ChAT-positive varicosities represented efferent presynaptic contacts, they should also express the proteins required for transmitter release. The synaptic proteins, synapsin I (SynI) and SV2, are present in efferent varicosities in a variety of species, yet absent from hair cell ribbon synapses, making them ideal efferent synaptic markers for our preparation (Safieddine and Wenthold, 1999; Zidanic, 2002; Holstein et al., 2005; Layton et al., 2005; Wibowo et al., 2009; Castellano-Muñoz et al., 2010). Consequently, we combined ChAT immunohistochemistry with labeling for SynI and SV2. In the turtle crista, SynI labeling appeared as small puncta concentrated along the basal half of the hair cell layer. Immunolabel for SynI extended the full length of the neuroepithelium from the torus (Fig. 4A) to the planum (not shown) where it overlapped with ChAT-positive varicosities (Fig. 4B). This suggested that ChAT-positive varicosities were, in fact, presynaptic release sites. As was the case with ChAT staining, occasional SynI-positive puncta were also visible in regions apical to nuclei of type II hair cells (arrows, Fig. 4A) as well as below the hair cell layer (arrowheads, Fig. 4A).

Interestingly, at higher magnifications, the localization of the SynI label was often skewed to one side of the varicosity (inset, Fig. 4B). One possible explanation was that this represented vesicle accumulation in the most distal portion of the efferent varicosity prior to synapsing on postsynaptic targets. The asymmetrical distribution of synaptic vesicles is seen in EM images of efferent terminals from turtle crista neuroepithelium (Holt et al., 2006). Three additional observations provided further support. First, similar staining patterns were observed when staining for ChAT and the synaptic vesicle protein SV2 (Fig. 4C, D). As with SynI, SV2 label was also localized to one side of ChAT-positive varicosities on both type II hair cells (arrowheads, Fig. 4C) and calyx-bearing afferents (arrowheads, Fig. 4D). Secondly, consistent with labeling the synaptic vesicle pool, SV2-positive puncta were directed towards the base of type II hair cells (Fig. 4C) and the axonal stalk of calyx-bearing afferents (Fig. 4D). Consistent with the reported literature, SynI or SV2 staining was not

seen in hair cells. Finally, triple-labeling experiments utilizing ChAT, SynI and SV2 demonstrated that nearly all ChAT-positive varicosities were co-labeled with both SynI and SV2 (Fig. 4E). Higher magnification images demonstrated that while ChAT label stained much of the varicosity, staining for SynI and SV2 were typically partitioned to one side and occupied the same footprint (Fig. 4E, right panels). There was also some suggestion that ChAT labeling was slightly more intense in the areas labeled with anti-SynI and anti-SV2.

In order to estimate the amount of overlap among these three efferent markers, a quantitative colocalization analysis was performed. Briefly, in single z-planes taken from confocal image stacks of tissues labeled for ChAT, SynI and SV2, regions of interest (ROI) were drawn around single ChAT-positive puncta and then we asked whether there was a correlation between the gray values of fluorescence intensity between the two signals (i.e. ChAT vs. SynI; ChAT vs. SV2 or SynI vs. SV2). From these gray values, a scatter plot was generated with a Pearson's correlation coefficient given for each puncta (Manders et al., 1992). In brief, the Pearson's correlation coefficient (PCC) is based on a linear scale of −1 to +1 with +1 indicating 100% colocalization, 0 for random overlap, and −1 indicating an inverse correlation between the gray values (fluorescence intensity) of the two channels (for more details see Costes et al., 2004 and Bolte and Cordelieres, 2006). Using this analysis we found that ChAT-positive puncta (n=57) were positively correlated with both SynI-positive and SV2-positive puncta (PCC = 0.656 ± 0.019 and 0.623 ± 0.022, respectively). SynI-positive and SV2-positive puncta were also positively correlated (PCC = 0.862 ± 0.019). Statistical significance was evaluated using a one-sample t-test (McDonald and Dunn, 2012). The PCC values from each of the three comparisons were significantly different from zero ($p<0.0001$). Higher correlation indices for SynI and SV2 are consistent with observations that both proteins occupy the same compartment (Fig 4E, right panels). Similar PCC values were also observed if we chose ROI's based upon SynI or SV2 signals instead of ChAT (data not shown). However, when comparable ROI's were drawn in regions without synaptic staining (i.e. in the hair cell layer outside of the synaptic zone), colocalization analyses generated PCC values (0.014 ± 0.014, 0.023 ± 0.014, and 0.019 ± 0.028 for ChAT vs SynI, ChAT vs SV2 or SynI vs SV2, respectively; n=57) that were not significantly different from zero ($p\geq0.1132$). Taken together our immunohistochemical data indicate that SynI and SV2 are reliable and robust efferent synaptic markers in turtle cristae where they colocalize with ChAT and each other.

CGRP is colocalized with ChAT in turtle efferent varicosities

The robust ChAT staining of vestibular efferent neurons in turtle cristae is in good agreement with the consensus that the predominant vestibular efferent transmitter is acetylcholine (ACh). However, the presence of dense core vesicles in efferent terminals in a number of species has been used to suggest a role for peptidergic transmission in the vestibular periphery. The most compelling evidence to date implicates calcitonin gene-related peptide (CGRP), a 37-amino acid neuropeptide frequently coexpressed at cholinergic synapses including the neuromuscular junction (NMJ) and auditory, lateral line, and vestibular efferent neurons (Adams et al., 1987; Sliwinska-Kowalska et al., 1989; Wackym et al., 1991; Lu et al., 1999; Cabanillas and Luebke, 2002; Luebke et al., 2014). We used immunohistochemistry with two CGRP antibodies to identify if CGRP was expressed in the

turtle cristae. In the turtle crista, staining for CGRP appeared as intense puncta scattered throughout the neuroepithelium (Fig. 5A). Similar CGRP staining was also evident in the turtle lagena, utricle, and saccule (data not shown). In whole mount preparations, CGRP staining was extensively colocalized with staining for ChAT (Fig. 5B). At higher magnifications, CGRP staining was present in ChAT-positive varicosities in the hair cell layer as well as in ChAT-positive fibers within the stroma (Fig. 5C–E). The deposition of CGRP label within efferent fibers and varicosities was less uniform than ChAT, instead appearing granulated (insets, Fig. 5C–E). This beaded pattern of CGRP staining also highlighted small efferent “tendrils” that projected through the hair cell layer (arrowhead, Figs. 5D, 5E). These extensions were previously unappreciated as ChAT staining within these same structures was typically quite faint (arrowhead, Fig. 5C). Further colocalization analyses was performed on individual z planes and indicated a high level of colocalization of CGRP and ChAT-positive puncta as demonstrated by a PCC of 0.507 ± 0.026 (n=52 puncta). Statistical significance was again evaluated using a one-sample t-test (McDonald and Dunn, 2012) that indicated that this PCC was significantly different from zero ($p<0.0001$). In the same z planes, the mean PCC value of comparable ROI’s drawn in adjacent regions without ChAT and CGRP label was not significantly different from zero ($p=0.8164$).

ChAT expression in Vestibular Tissues of Zebra Finch and Mouse

In order to support the specificity of vestibular efferent markers in turtle, vestibular end organs from songbird and mouse were also procured and processed for ChAT, Myo7A, calretinin, and the synaptic markers SV2, SynI and Syntaxin (Figs. 6, 7). Antibodies to syntaxin were used as an alternative presynaptic marker in lieu of antibodies to SynI that failed to label efferent terminals in bird. ChAT immunostaining of bird and mouse crista revealed similar efferent innervation patterns as we observed in turtle tissue (Figs. 6A, 7A, and 7D). In particular, ChAT-positive fibers, after extensive branching at the hair cell-supporting cell junction, heavily innervated the hair cell layer throughout the crista. Double labeling experiments with ChAT and Myo7A showed an abundance of ChAT-positive puncta along the basal portions of hair cells in both bird (Fig. 6B) and mouse (Fig. 7C–E). However, in contrast to turtle, ChAT-positive varicosities on type II hair cells along regions apical to the nucleus were more commonly found in both bird and mouse crista, while in turtle these types of varicosities were much less frequently observed (Figs. 6B, 7E). Also, in contrast to turtle crista where Myo7A label appeared to be distributed evenly throughout the entirety of the hair cell, Myo7A staining in bird and mammal was more concentrated at the hair cell cuticular plate (Figs. 6B, 7E).

ChAT-positive fibers in mouse and bird traversed across the tissue in a more diffuse pattern than in turtle. In 40μm longitudinal sections from turtle, an observer could frequently trace the full length of a ChAT-positive fiber from where it entered the stroma to its termination in the apical portion of the sensory epithelia (Fig. 1D). In contrast, in bird and mammal, ChAT-positive fibers could often be traced only a portion of the distance from stroma to apex where upon they coursed too deeply into the tissue (and presumably into the next tissue section) before re-appearing near the hair cell-supporting cell layer and terminating along hair cells and afferents. Alternatively, they may undergo earlier branching in the stroma

making it difficult to follow their course. Consequently, using our current methods, imaging the entire length of whole ChAT-positive fibers in bird and mouse was frequently not possible creating some uncertainty in tabulating reliable or accurate efferent fiber counts in mouse and bird needed for comparison to turtle.

Calretinin and Efferent Synaptic Markers in Zebra Finch and Mouse

Similar to turtle cristae, ChAT and calretinin labeled distinct, anatomically separate fiber populations in both bird and mouse cristae. In zebra finch cristae, calretinin showed a similar labeling pattern as turtle cristae with strong staining of calyx bearing afferents across the central zone and more diffuse staining of type II hair cells in the planum region (Fig. 6C). Bouton afferents near the apex were less prominent. In bird, we also observed that the central zone, where calretinin-positive calyces were located, appeared to be somewhat more expansive than what we observed in turtle with calretinin-positive calyces in bird often being located along regions closer to the planum. The overall shape of the bird posterior crista was also more “W” shaped than what we observed in either turtle or mouse with a strong curvature of the central zone adjacent to a deeply sloped apex and planum regions (Fig. 6, see also Masetto and Correia, 1997). In our hands, as reported previously in mouse (Desai et al., 2005a,b), antibodies against calretinin strongly labeled calyx-only afferents in the central zone of mouse crista (Fig. 7F, 7H) as well as hair cells in the utricle (data not shown). Some crista hair cells were also faintly stained with calretinin but we did not determine if they were type I or type II. In both bird and mouse, ChAT-positive varicosities did not appear to aggregate along the axonal stalk at least to the extent seen in turtle. They were, however, scattered along the outer face of calyceal endings (Figs. 6C, 7F).

In bird cristae, labeling with antibodies against the synaptic markers syntaxin and SV2 labeled a plethora of synaptic structures primarily located along calretinin-positive calyces (Fig. 6D) and along the base of the hair cell layer (Fig. 6E, F). The distribution of puncta labeled by SV2 and syntaxin mirrored that of ChAT-positive varicosities. Syntaxin staining was more abundant within the neuroepithelium than SV2 staining which is consistent with the presence of syntaxin at both afferent and efferent synapses (Hennig and Cotanche 1998; Safieddine and Wenthold, 1999; Demêmes et al., 2001; Nouvian et al., 2011). Although several antibodies were tested, SynI immunostaining in our hands was noticeably absent from songbird vestibular tissue.

Synapsin I staining in mouse canal cristae showed a similar staining pattern as that seen in turtle with many SynI-positive puncta located along the base of the hair cell layer (Fig. 7G, 7H). High resolution, zoomed confocal images demonstrate the presence of SV2-positive and SynI-positive puncta terminating along the outer face of calretinin-positive calyces in bird and mouse, respectively (Figs. 6D, 7I). In contrast to turtle, SV2-positive and SynI-positive puncta were frequently noted along more central and apical portions of calretinin-positive calyces in both bird and mouse vestibular tissues, respectively (Figs. 6D, 7I).

Efferent Fiber Diameter Estimates in Turtle, Bird and Mouse

The specificity of ChAT fiber labeling was further confirmed in ChAT and calretinin co-labeling experiments. In turtle, bird, and mouse, we simply compared fiber diameters of

calretinin-positive fibers versus ChAT-positive fibers. Measurements of ChAT-positive fibers were pooled from across the sensory epithelia of each species, as their diameter did not differ depending upon region sampled (data not shown). A two-way ANOVA of fiber diameter vs. species revealed that calretinin-positive fibers were significantly larger in diameter than ChAT-positive fibers in the same species (Fig. 8). There was a main effect of fiber type $F(1,54) = 92.7$, $p<0.0001$ and of species $F(2,54) = 17.2$, $p<0.0001$ with a significant interaction $F(2,54) = 5.2$, $p<0.0001$ between these two factors. Post hoc tests showed that in each species, calretinin-positive afferent fibers were significantly greater in size than ChAT-positive fibers ($t(18) = 5.6$, 8.7, and 13.0, $p<0.0001$ for mouse, turtle, and bird, respectively) with fiber diameter measurements of 2.89 ± 0.21 vs. 1.36 ± 0.07 μm in mouse, 4.02 ± 0.18 vs. 1.65 ± 0.09 μm for turtle, and 5.75 ± 0.34 vs. 2.19 ± 0.13 μm for bird (calretinin vs. ChAT fiber diameter, mean ± SEM; n= 10 for each species). Further post hoc analysis showed that across species, calretinin-positive fibers were significantly different in fiber diameter (bird > turtle, $t(18) = 6.326$, $p<0.0001$; turtle > mouse, $t(18) = 4.133$, $p<0.001$; bird > mouse, $t(18) = 10.46$, $p<0.0001$) while ChAT-positive fibers were only different in diameter size between bird and mouse ($t(18) = 3.033$, $p<0.05$). Together this data demonstrate a significant difference in fiber diameter width when comparing ChAT-positive efferent fibers vs. calretinin-positive afferent fibers within each species.

DISCUSSION

Large networks of afferent and efferent fibers are known to innervate the vestibular end organs of vertebrates. Within each end organ, afferent fibers are typically larger in diameter, and give rise to bouton and/or calyx processes that form glutamatergic synapses with hair cells while efferent fibers are smaller in diameter, predominantly cholinergic, and synapse upon hair cells and afferent processes (Lysakowski and Goldberg, 2004). Using standard immunohistochemical procedures, we exploited some of these anatomical and biochemical differences to distinguish efferent fibers and their varicosities in the peripheral vestibular system of turtle, bird and mouse. In this study, we have confirmed the presence of a robust efferent innervation in all three species that was previously not appreciated. Data here demonstrate that this system is highly conserved across species yet some of the individual synaptic proteins involved in efferent synaptic release may differ.

Cholinergic vestibular efferent neurons innervate type II hair cells and afferent processes

Antibodies to the enzyme choline acetyltransferase (ChAT) have been commonly used to label efferent cholinergic fibers and varicosities in the inner ear of several species (Kong et al., 1994A, 1994B, 2002; Wibowo et al, 2009). Since ChAT is synthesized in the cell body and transported to the varicosities via axonal transport (Oda, 1999), we expected to find ChAT labeling in both efferent fibers and efferent varicosities in the vestibular periphery. In our hands, labeling for ChAT emphasized a broad system of efferent fibers coursing through the stroma to end as varicosities across the sensory epithelia in each of the three species studied. ChAT-positive varicosities were primarily concentrated along the basal half of the hair cell layer, but were also occasionally identified along the apical reaches of the epithelium as well as within the supporting cell layer. Furthermore, apical efferent varicosities in turtle were further accentuated by co-labeling for CGRP. In each species

examined here, approximately two to five ChAT-positive varicosities were identified on most type II hair cells, consistent with dissector counts in both chinchilla and squirrel monkey (Lysakowski and Goldberg, 1997, 2008).

ChAT-positive varicosities were routinely found adjacent to the terminal portions of both calyx-bearing (i.e. calyx/dimorphic, CD) and bouton vestibular afferents. In turtle CD afferents, many varicosities were also clustered along the afferent axonal stalk just below the calyceal expansion as well as along the outer face of the calyx terminal. In bird and mouse, although efferent varicosities on the calyx terminal within the hair cell layer were common, clustering along the axonal stalk was much less pronounced. Efferent-mediated excitation of CD afferents is quite similar in turtle and mammals with respect to response amplitude, kinetics, and duration (Goldberg and Fernandez, 1980; Brichta and Goldberg, 2000b; Marlinski et al. 2004; Holt et al. 2006; Jordan et al., 2013). It is therefore somewhat interesting in how efferent synapses cluster along the axonal stalk of calyx-bearing afferents in turtle, while in mouse and bird tissues, efferent synapses were found along the outer face of calyceal endings with very few along the stalk itself. What might be more telling is the proximity of these efferent synapses in both species to the spike initiation site and different ionic channel domains within the CD ending (Lysakowksi et al., 2011). Perhaps, it is these spatial relationships that preserve similarities in the response of CD afferents to efferent stimulation between turtle and mammals.

In order to further support that ChAT label was specifically confined to efferent but not afferent fibers, we double labeled for the calcium-binding protein calretinin and ChAT in a subset of vestibular canal sections from turtle, bird, and mouse. Calretinin has been shown to label calyx afferents as well as type I and type II vestibular hair cells in turtle and rodents (Monk and Peterson, 1995; Leonard and Kevetter, 2002; Desai et al., 2005a, b; Simmons et al., 2010; Huwe et al., 2011). In the current study, we show that calretinin-positive afferent fibers in turtle, bird and mouse vestibular sensory epithelia were distinct from those that labeled with antibodies to ChAT. Calretinin-positive fibers were large-diameter and were located primarily in the central zone where they formed calyceal terminals. In contrast, ChAT-positive fibers were relatively thin and found distributed across the epithelia where they ended on both hair cells and afferents including calretinin-positive afferents. Unlike reports in rodents (Leonard and Kevetter, 2002; Desai et al., 2005a, b), antibodies to calretinin also labeled bouton afferents in turtle and bird immediately outside of the central zone near the torus or apex, respectively.

Although our primary motivation in immunostaining for calretinin was to label afferent fibers, we did also observe calretinin expression in hair cells in all three species. Interestingly, in turtle and bird, calretinin-positive type II hair cells were always located near the planum region of both species suggesting that type II hair cells across the epithelia may also be further divided into calretinin-positive or negative groups. There was no obvious type I hair cells stained for calretinin in either turtle or bird cristae. Desai et al., (2005b) utilized a flattened whole mount epithelial preparation to determine that a small percentage of type I hair cells (~5%) and ~20% of type II hair cells in mouse and rat crista were calretinin-positive. Although some mouse crista hair cells in our sections were stained with

calretinin, we did not further resolve if they were type I or type II nor try to quantify their numbers.

ChAT routinely labeled small diameter fibers in turtle, bird and mouse that were a separate population from the large diameter calretinin-positive afferent fibers. In regards to ChAT-positive fiber diameter, all species were quite similar in size with an average diameter of ~1.36 μm for mice, ~1.65 μm for turtles and ~2.19 μm for birds. These values are in range for previous efferent fiber measurements. Fish vestibular efferents were estimated to be around ~1.4 μm in diameter (Mensinger and Highstein, 1999) while HRP-labeled efferent fibers in turtle were reported to be ~1.37 μm (Fayyazuddin et al., 1991). Statistically, when comparing efferent fiber diameter, only birds and mice were slightly, but significantly different from each other ($p < 0.05$), while turtle efferent fiber diameters were not different from bird or mouse. In comparing the two fiber groups, ChAT-positive efferents were significantly different in diameter size than calretinin-positive afferents in the same species ($p<0.0001$). On average, ChAT-positive fibers were 2.1–2.6 times smaller in diameter than calretinin-positive fibers in the vestibular end organs of the three species studied. It is important to note, however, that calretinin-positive afferents are likely to be the largest of the afferents present in the crista and do not encompass afferent fiber population in full (Lysakowski et al., 1999).

Localization and expression of efferent presynaptic markers

Antibodies to the synaptic vesicle proteins, synapsin I (SynI) and SV2, were employed in the current study to facilitate identification of presynaptic efferent varicosities in the vestibular periphery. The rationale behind choosing these antibodies was that these two synaptic proteins are commonly expressed by inner ear efferents, but are not a component of the release machinery in hair cells (Favre et al., 1986; Saffeidine and Wenthold, 1999; Zidanic, 2002; Holstein et al., 2005; Layton et al., 2005; Wibowo et al., 2009; Castellano-Muñoz et al., 2010). In turtle, antibodies to both SynI and SV2 were shown to co-label with ChAT-positive efferent varicosities. Furthermore, using single plane confocal images, a high level of colocalization was found among ChAT, SynI, and SV2 in efferent varicosities in turtle cristae. The expression of these proteins should mirror the distribution of synaptic vesicles. In turtle, SynI and SV2 label were often localized to the side of the varicosities closest to the presumed synaptic cleft as has been seen in other neural preparations (De Camilli et al., 1983; Chakkalakal et al., 2010; Bragina et al., 2013). This polarized distribution was helpful in identifying the postsynaptic cellular target.

Unlike turtle, labeling for SynI was not observed in the peripheral vestibular end organs of Zebra Finch. The lack of SynI staining may be explained by a previous report stating that a homologue of the SynI gene may be lacking in songbirds and chickens (Velho and Mello, 2008). Previous reports of synapsin II (Syn II) antigenicity within brain tissue of songbirds (Pinaud et al., 2008; Velho and Mello, 2008) suggested that Syn II might be a good candidate as a pre-synaptic marker in bird vestibular tissue. Unfortunately, in our hands, none of the several commercially available SynI antibodies or a Syn II antibody, with reported staining in bird auditory forebrain (Pinaud et al., 2008), was effective at labeling efferent varicosities within the bird vestibular epithelia. Two other synaptic markers, SV2

and syntaxin, however, did label punctate structures along the base of hair cells and afferents in the songbird crista. In contrast, immunoreactivity for SynI, but not for syntaxin or SV2, were visualized in mouse vestibular tissue. The lack of SV2 or syntaxin staining might be attributed to the difficulty in utilizing monoclonal antibodies in mouse tissues. An alternative explanation, aside from antigenicity issues, is that the lack of immunoreactivity among these different presynaptic markers in bird and mouse might also suggest that vestibular efferents among the three species utilize different presynaptic machinery.

Defining the efferent synapse through pre- and postsynaptic markers

Although the synaptic mechanisms underlying afferent responses to efferent stimulation in birds and mammals have not been worked out, pharmacological data in turtle has shown that the release of ACh during efferent stimulation activates α9α10 nicotinic acetylcholine receptors (α9α10 nAChRs) on type II hair cells and α4β2-containing nAChRs on bouton and calyx/dimorphic afferent processes (Holt et al., 2006; Jordan et al., 2013). Visualizing the relative abundance of efferent synapses on hair cells and vestibular afferents as well as the density of these postsynaptic receptor mechanisms should be helpful in understanding the diversity in afferent responses to efferent stimulation across the vertebrate scale. As a first pass, we evaluated the relative density of ChAT-positive varicosities among the planum, central, and torus regions of the turtle crista. Here, the mean number of varicosities per 400 μm^2 was 6.67, 8.28 and 9.44, respectively. The torus values are similar to the recently reported density of ChAT-positive varicosities in the mouse crista (11.3 varicosities per 400 μm^2; Luebke et al., 2014). Furthermore, we have also demonstrated in turtle that there are significantly fewer ChAT-positive varicosities in the planum as compared to the torus. The lower number of efferent varicosities in the planum, in fact, may contribute to the smaller excitatory response of BP afferents to efferent stimulation (Brichta and Goldberg, 2000b). But other factors such as release efficacy of efferent transmitter (e.g. ACh), postsynaptic receptor density, and differences in afferent sensitivity should also be investigated. An estimation of the mean number of ChAT-positive varicosities per hair cell or afferent across the different regions should also provide some insight into whether decreases in the density of ChAT-positive varicosities are necessarily associated with a reduction in efferent input.

The presynaptic markers used in this study (i.e. SynI, SV2, and syntaxin) were instructive in indicating which ChAT-positive varicosities likely represented efferent release sites. We have assumed that these release sites were functional given their direct apposition to hair cells and afferent processes, but such assumption also requires the identification of an adjacent postsynaptic receptor complex. This would include labeling cholinergic receptors, downstream effectors, and/or proteins involved in receptor clustering. Labeling of afferent and efferent postsynaptic structures has been successfully used in the cochlea (Khimich et al., 2005; Osman et al., 2008; Liberman et al., 2011; Roux et al., 2011). However, studies pairing and localizing efferent pre- and postsynaptic targets in the peripheral vestibular system are lacking. This is further complicated by the lack of good antibodies for cholinergic receptors (Moser et al., 2007; Jositsch et al., 2009). A few studies have successfully used fluorescently-labeled α-bungarotoxin, as well as antibodies against proteins involved in nAChR clustering and assembly, to identify the postsynaptic receptor

domain in vestibular tissue (Ishiyama et al., 1995; Dailey et al., 2000; Osman et al., 2008). What remains is to combine reliable postsynaptic markers with simultaneous labeling of the presynaptic compartment in order to better understand the organization of vestibular efferent synapses.

Acknowledgments

Acknowledgement of Support: This work was supported by NIH/NIDCD grants R01DC008981 (JCH), and P30-DC005409 (CNCS - Center for Communicative and Navigational Sciences, University of Rochester).

This work was supported by NIH/NIDCD grants R01DC008981 (JCH), and P30-DC005409 (CNCS - Center for Communicative and Navigational Sciences, University of Rochester). We would also like to thank Lila Yang and Sarah Westendorf for help in tissue acquisition and Linda Callahan in the URMC Confocal and Conventional Microscopy Core (RRID: SciEx_12080) for her help in acquisition of immunohistochemical images. Dr. Anna Lysakowski commented on a previous version of the manuscript.

LITERATURE CITED

Adams JC, Mroz EA, Sewell WF. A possible neurotransmitter role for CGRP in a hair-cell sensory organ. Brain Res. 1987; 419:347–351. [PubMed: 2890408]

Anadón R, Molist P, Rodríguez-Moldes I, López JM, Quintela I, Cerviño MC, Barja P, González A. Distribution of choline acetyltransferase immunoreactivity in the brain of an elasmobranch, the lesser spotted dogfish (Scyliorhinus canicula). J Comp Neurol. 2000; 420:139–170. [PubMed: 10753304]

Balaban CD. Vestibular nucleus projections to the Edinger-Westphal and anteromedian nuclei of rabbits. Brain Res. 2003; 963(1–2):121–31. [PubMed: 12560117]

Barnstable CJ, Hofstein R, Akagawa K. A marker of early amacrine cell development in rat retina. Brain Res. 1985; 352:286–290. [PubMed: 3896407]

Bergeron AL, Schrader A, Yang D, Osman AA, Simmons DD. The final stage of cholinergic differentiation occurs below inner hair cells during development of the rodent cochlea. J Assoc Res Otolaryngol. 2005; 6:401–415. [PubMed: 16228856]

Bernard C, Cochran SL, Precht W. Presynaptic actions of cholinergic agents upon the hair cell-afferent fiber synapses in the vestibular labyrinth of the frog. Brain Res. 1985; 338:225–236. [PubMed: 2992685]

Boëda B, Weil D, Petit C. A specific promoter of the sensory cells of the inner ear defined by transgenesis. Hum Mol Genet. 2001; 10(15):1581–9. [PubMed: 11468276]

Bolte S, Cordelieres FP. A guided tour into subcellular colocalization and analysis in light microscopy. J Microsc. 2006; 224:213–232. [PubMed: 17210054]

Bragina L, Fattorini G, Giovedí S, Melone M, Bosco F, Benfenati F, Conti F. Analysis of Synaptotagmin, SV2, and Rab3 Expression in Cortical Glutamatergic and GABAergic Axon Terminals. Front Cell Neurosci. 2012; 5:32. [PubMed: 22275882]

Brichta AM, Petersen EH. Functional architecture of vestibular primary afferents from the posterior semicircular canal of a turtle, *Pseudemys (Trachemys) scripta elegans*. J Comp Neurol. 1994; 344:481–507. [PubMed: 7929889]

Brichta AM, Goldberg JM. Morphological identification of physiologically characterized afferents innervating the turtle posterior crista. J Neurophysiol. 2000a; 83:1202–1223. [PubMed: 10712450]

Brichta AM, Goldberg JM. Responses to efferent activation and excitatory response-intensity relations of turtle posterior-crista afferents. J Neurophysiol. 2000b; 83:1224–42. [PubMed: 10712451]

Brooke RE, Corns L, Edwards IJ, Deuchars J. Kv3.3 immunoreactivity in the vestibular nuclear complex of the rat with focus on the medial vestibular nucleus: targeting of Kv3.3 neurones by terminals positive for vesicular glutamate transporter 1. Brain Res. 2010; 1345:45–58. [PubMed: 20471378]

Bruce G, Wainer BH, Hersh LB. Immunoaffinity purification of human choline acetyltransferase: comparison of the brain and placental enzymes. J Neurochem. 1985; 45(2):611–20. [PubMed: 4009177]

Buckley K, Kelly RB. Identification of a transmembrane glycoprotein specific for secretory vesicles of neuronal and endocrine cells. J Cell Biol. 1985; 100:1284–1294. [PubMed: 2579958]

Cabanillas LA, Luebke AE. CGRP- and cholinergic-containing fibers project to guinea pig outer hair cells. Hear Res. 2002; 172:14–17. [PubMed: 12361863]

Castellano-Muñoz M, Israel SH, Hudspeth AJ. Efferent control of the electrical and mechanical properties of hair cells in the bullfrog's sacculus. PLoS One. 2010; 5:e13777. [PubMed: 21048944]

Chakkalakal JV, Nishimune H, Ruas JL, Spiegelman BM, Sanes JR. Retrograde influence of muscle fibers on their innervation revealed by a novel marker for slow motoneurons. Development. 2010; 137:3489–3499. [PubMed: 20843861]

Costes SV1, Daelemans D, Cho EH, Dobbin Z, Pavlakis G, Lockett S. Automatic and quantitative measurement of protein-protein colocalization in live cells. Biophys J. 2004; 86:3993–4003. [PubMed: 15189895]

Dailey SH, Wackym PA, Brichta AM, Gannon PJ, Popper P. Topographic distribution of nicotinic acetylcholine receptors in the cristae of a turtle. Hear Res. 2000; 141:51–56. [PubMed: 10713495]

De Camilli P, Cameron R, Greengard P. Synapsin I (protein I), a nerve terminal-specific phosphoprotein. I. Its general distribution in synapses of the central and peripheral nervous system demonstrated by immunofluorescence in frozen and plastic sections. J Cell Biol. 1983; 96:1337–1354. [PubMed: 6404910]

Dechesne CJ, Rabejac D, Desmadryl G. Development of calretinin immunoreactivity in the mouse inner ear. J Comp Neurol. 1994; 346:517–529. [PubMed: 7983242]

Demêmes D, Dechesne CJ, Venteo S, Gaven F, Raymond J. Development of the rat efferent vestibular system on the ground and in microgravity. Brain Res Dev Brain Res. 2001; 128:35–44.

Desai SS, Ali H, Lysakowski A. Comparative morphology of rodent vestibular periphery. II. Cristae ampullares. J Neurophysiol. 2005b; 93:267–280. [PubMed: 15240768]

Desai SS, Zeh C, Lysakowski A. Comparative morphology of the rodent vestibular periphery: I. Saccular and utricular maculae. J Neurophysiol. 2005a; 93:251–266. [PubMed: 15240767]

Dickman JD, Correia MG. Bilateral communication between vestibular labyrinths in pigeons. Neuroscience. 1993; 57:1097–1108. [PubMed: 8309545]

Duncan LJ, Mangiardi DA, Matsui JI, Anderson JK, McLaughlin-Williamson K, Cotanche DA. Differential expression of unconventional myosins in apoptotic and regenerating chick hair cells confirms two regeneration mechanisms. J Comp Neurol. 2006; 499(5):691–701. [PubMed: 17048225]

Favre D, Scarfone E, Di Gioia G, De Camilli P, Dememes D. Presence of synapsin I in afferent and efferent nerve endings of vestibular sensory epithelia. Brain Res. 1986; 384:379–782. [PubMed: 3096490]

Fayyazuddin A, Brichta AM, Art JJ. Organization of eighth nerve efferents in the turtle, *Pseudemys scripta*. Soc Neurosci Abstr. 1991; 17:312.

Goldberg JM, Fernández C. Efferent vestibular system in the squirrel monkey: anatomical location and influence on afferent activity. J Neurophysiol. 1980; 43:986–1025. [PubMed: 6767000]

Hackney CM, Mahendrasingam S, Jones EM, Fettiplace R. The distribution of calcium buffering proteins in the turtle cochlea. J Neurosci. 2003 Jun 1; 23(11):4577–89. [PubMed: 12805298]

Hasson T, Heintzelman MB, Santos-Sacchi J, Corey DP, Mooseker MS. Expression in cochlea and retina of myosin VIIa, the gene product defective in Usher 1B. Proc Natl Acad Sci USA. 1995; 92:9815–9819. [PubMed: 7568224]

Hasson T, Gillespie PG, Garcia JA, MacDonald RB, Zhao Y, Yee AG, Mooseker MS, Corey DP. Unconventional myosins in inner-ear sensory epithelia. J Cell Biol. 1997; 137(6):1287–307. [PubMed: 9182663]

Hennig AK, Cotanche DA. Regeneration of cochlear efferent nerve terminals after gentamycin damage. J Neurosci. 1998; 18:3282–3296. [PubMed: 9547237]

Highstein SM, Baker R. Action of the efferent vestibular system on primary afferents in the toadfish, *Opsanus tau*. J Neurophysiol. 1985; 54:370–384. [PubMed: 4031993]

Holstein GR, Martinelli GP, Boyle R, Rabbitt RD, Highstein SM. Ultrastructural observations of efferent terminals in the crista ampullaris of the toadfish, *Opsanus tau*. Exp Brain Res. 2004; 157:128–136. [PubMed: 15318400]

Holstein G, Martinelli G, Nicolae R, Rosenthal T, Friedrich V. Synapsin-like immunoreactivity is present in hair cells and efferent terminals of the toadfish crista ampullaris. Exp Brain Res. 2005; 162:287–292. [PubMed: 15599720]

Holt JC, Lysakowski A, Goldberg JM. Mechanisms of efferent-mediated responses in the turtle posterior crista. J Neurosci. 2006; 26:13180–13193. [PubMed: 17182768]

Huwe J, Williams B, Rowe M, Peterson E. Afferent Terminal Arbor Structure in Turtle Utricle ARO abstracts. 2011

Inoue A, Obata K, Akagawa K. Cloning and sequence analysis of cDNA for a neuronal cell membrane antigen, HPC-1. J Biol Chem. 1992; 267:10613–10619. [PubMed: 1587842]

Ishiyama A, Lopez I, Wackym PA. Distribution of efferent cholinergic terminals and alpha-bungarotoxin binding to putative nicotinic acetylcholine receptors in the human vestibular end-organs. Laryngoscope. 1995; 105:1167–1172. [PubMed: 7475869]

Johnson CD, Epstein ML. Monoclonal antibodies and polyvalent antiserum to chicken choline acetyltransferase. J Neurochem. 1986; 46:968–976. [PubMed: 3512775]

Jordan PM, Parks XX, Contini D, Holt JC. A review of synaptic mechanisms of vestibular efferent signaling in turtles: extrapolation to efferent actions in mammals. J Vestib Res. 2013; 23:161–75. [PubMed: 24177348]

Jositsch G, Papadakis T, Haberberger RV, Wolff M, Wess J, Kummer W. Suitability of muscarinic acetylcholine receptor antibodies for immunohistochemistry evaluated on tissue sections of receptor gene-deficient mice. Naunyn Schmiedebergs Arch Pharmacol. 2009; 379:389–395. [PubMed: 18974978]

Khimich D, Nouvian R, Pujol R, Tom Dieck S, Egner A, Gundelfinger ED, Moser T. Hair cell synaptic ribbons are essential for synchronous auditory signalling. Nature. 2005; 434:889–894. [PubMed: 15829963]

Kong WJ, Egg G, Hussl B, Seyr M, Schrott-Fischer A. A study of neurotransmitters in human inner ear. Preservation of human temporal bone and value of organ donation for inner ear research. Acta Otolaryngol. 1994a; 114:245–253. [PubMed: 7915484]

Kong WJ, Egg G, Hussl B, Spoendlin H, Schrott-Fischer A. Localization of chat-like immunoreactivity in the vestibular endorgans of the rat. Hear Res. 1994b; 75:191–200. [PubMed: 8071146]

Kong WJ, Hussl B, Thumfart WF, Schrott-Fischer A. Ultrastructural localization of ChAT-like immunoreactivity in the human vestibular periphery. Hear Res. 1998; 119:96–103. [PubMed: 9641322]

Kong WJ, Scholtz AW, Hussl B, Kammen-Jolly K, Schrott-Fischer A. Localization of efferent neurotransmitters in the inner ear of the homozygous Bronx waltzer mutant mouse. Hear Res. 2002; 167(1–2):136–55. [PubMed: 12117537]

Kopeikina KJ, Polydoro M, Tai HC, Yaeger E, Carlson GA, Pitstick R, Hyman BT, Spires-Jones TL. Synaptic alterations in the rTg4510 mouse model of tauopathy. J Comp Neurol. 2013; 5216:1334–1353. [PubMed: 23047530]

Kubke MF, Massoglia DP, Carr CE. Developmental changes underlying the formation of the specialized time coding circuits in barn owls (*Tyto alba*). J Neurosci. 2002; (17):7671–9. [PubMed: 12196590]

Layton MG, Robertson D, Everett AW, Mulders WH, Yates GK. Cellular localization of voltage-gated calcium channels and synaptic vesicle-associated proteins in the guinea pig cochlea. J Mol Neurosci. 2005; 27:225–244. [PubMed: 16186634]

Lee EJ, Merwine DK, Padilla M, Grzywacz NM. Choline acetyltransferase-immunoreactive neurons in the retina of normal and dark-reared turtle. J Comp Neurol. 2007; 503:768–778. [PubMed: 17570494]

Leijon S, Magnusson AK. Physiological characterization of vestibular efferent brainstem neurons using a transgenic mouse model. PLoS One. 2014; 9(5):e98277. [PubMed: 24867596]

Leonard RB, Kevetter GA. Molecular probes of the vestibular nerve. I. Peripheral termination patterns of calretinin, calbindin and peripherin containing fibers. Brain Res. 2002; 928:8–17. [PubMed: 11844467]

Li GQ, Kevetter GA, Leonard RB, Prusak DJ, Wood TG, Correia MJ. Muscarinic acetylcholine receptor subtype expression in avian vestibular hair cells, nerve terminals and ganglion cells. Neuroscience. 2007; 146:384–402. [PubMed: 17391855]

Liberman LD, Wang H, Liberman MC. Opposing gradients of ribbon size and AMPA receptor expression underlie sensitivity differences among cochlear-nerve/hair-cell synapses. J Neurosci. 2011; 31:801–808. [PubMed: 21248103]

Liu W, Davis RL. Calretinin and calbindin distribution patterns specify subpopulations of type I and type II spiral ganglion neurons in postnatal murine cochlea. J Comp Neurol. 522:2299–2318. [PubMed: 24414968]

Lopez IA, Acuna D, Beltran-Parrazal L, Espinosa-Jeffrey A, Edmond J. Oxidative stress and the deleterious consequences to the rat cochlea after prenatal chronic mild exposure to carbon monoxide in air. Neuroscience. 2008; 151:854–67. [PubMed: 18155845]

Lu JT, Son YJ, Lee J, Jetton TL, Shiota M, Moscoso L, Niswender KD, Loewy AD, Magnuson MA, Sanes JR, Emeson RB. Mice lacking alpha-calcitonin gene-related peptide exhibit normal cardiovascular regulation and neuromuscular development. Mol Cell Neurosci. 1999; 14:99–120. [PubMed: 10532808]

Luebke AE, Holt JC, Jordan PM, Wong YS, Caldwell JS, Cullen KE. Loss of α-Calcitonin Gene-Related Peptide (αCGRP) Reduces the Efficacy of the Vestibulo-ocular Reflex (VOR). J Neurosci. 2014; 34:10453–10458. [PubMed: 25080603]

Luebke AE, Maroni PD, Guth SM, Lysakowski A. Alpha-9 nicotinic acetylcholine receptor immunoreactivity in the rodent vestibular labyrinth. J Comp Neurol. 2005; 492:323–333. [PubMed: 16217793]

Lysakowski A. Synaptic organization of the crista ampullaris in vertebrates. Ann N Y Acad Sci. 1996; 781:164–182. [PubMed: 8694413]

Lysakowski A, Gaboyard-Niay S, Calin-Jageman I, Chatlani S, Price SD, Eatock RA. Molecular microdomains in a sensory terminal, the vestibular calyx ending. J Neurosci. 2011; 31:10101–10114. [PubMed: 21734302]

Lysakowski A, Goldberg JM. A regional ultrastructural analysis of the cellular and synaptic architecture in the chinchilla cristae ampullares. J Comp Neurol. 1997; 389:419–443. [PubMed: 9414004]

Lysakowski A, Alonto A, Jacobson L. Peripherin immunoreactivity labels small diameter vestibular 'bouton' afferents in rodents. Hear Res. 1999; 133(1–2):149–54. [PubMed: 10416873]

Lysakowski, A.; Goldberg, JM. Morphophysiology of the vestibular periphery. In: Highstein, SM.; Popper, A.; Fay, RR., editors. The vestibular system. Springer; New York: 2004. p. 57-152.

Lysakowski A, Goldberg JM. Ultrastructural analysis of the cristae ampullares in the squirrel monkey *(Saimiri sciureus)*. J Comp Neurol. 2008; 511:47–64. [PubMed: 18729176]

Marlinski V, Plotnik M, Goldberg JM. Efferent actions in the chinchilla vestibular labyrinth. J Assoc Res Otolaryngol. 2004; 5:126–143. [PubMed: 15357416]

Mandell JW, Townes-Anderson E, Czernik AJ, Cameron R, Greengard P, De Camilli P. Synapsins in the vertebrate retina: absence from ribbon synapses and heterogeneous distribution among conventional synapses. Neuron. 1990; 5(1):19–33. [PubMed: 2114884]

Manders EMM, Stap J, Brakenhoff GJ, Vandriel R, Aten JA. Dynamics of three-dimensional replication patterns during the s-phase, analyzed by double labeling of DNA and confocal microscopy. J Cell Sci. 1992; 103:857–862. [PubMed: 1478975]

Masetto S, Correia MJ. Electrophysiological properties of vestibular sensory and supporting cells in the labyrinth slice before and during regeneration. J Neurophysiol. 1997

McDonald JH, Dunn KW. Statistical tests for measures of colocalization in biological microscopy. J Microsc. 2012; 252:295–302. [PubMed: 24117417]

Mensinger AF, Highstein SM. Characteristics of regenerating horizontal semicircular canal afferent and efferent fibers in the toadfish, *Opsanus tau*. J Comp Neurol. 1999; 410:653–676. [PubMed: 10398055]

Meredith GE. Comparative view of the central organization of afferent and efferent circuitry for the inner ear. Acta Biol Hung. 1988; 39:229–245. [PubMed: 3077006]

Monk G, Peterson EH. Calretinin is not specific for calyceal afferents in the semicircular canals of Pseudemys scripta. Soc Neurosci Abstr. 1995; 21:918.

Moser N, Mechawar N, Jones I, Gochberg-Sarver A, Orr-Urtreger A, Plomann M, Salas R, Molles B, Marubio L, Roth U, Maskos U, Winzer-Serhan U, Bourgeois JP, Le Sourd AM, De Biasi M, Schröder H, Lindstrom J, Maelicke A, Changeux JP, Wevers A. Evaluating the suitability of nicotinic acetylcholine receptor antibodies for standard immunodetection procedures. J Neurochem. 2007; 102:479–492. [PubMed: 17419810]

Nouvian R, Neef J, Bulankina AV, Reisinger E, Pangršič T, Frank T, Sikorra S, Brose N, Binz T, Moser T. Exocytosis at the hair cell ribbon synapse apparently operates without neuronal SNARE proteins. Nat Neurosci. 2011; 14:411–413. [PubMed: 21378973]

Oda Y. Choline acetyltransferase: the structure, distribution and pathologic changes in the central nervous system. Pathol Intl. 1999; 49:921–937.

Ohno K, Takeda N, Kiyama H, Kato H, Fujita S, Matsunaga T, Tohyama M. Synaptic contact between vestibular afferent nerve and cholinergic efferent terminal: its putative mediation by nicotinic receptors. Brain Res Mol Brain Res. 1993; 18:343–346. [PubMed: 8326830]

Osman AA, Schrader AD, Hawkes AJ, Akil O, Bergeron A, Lustig LR, Simmons DD. Muscle-like nicotinic receptor accessory molecules in sensory hair cells of the inner ear. Mol Cell Neurosci. 2008; 38:153–169. [PubMed: 18420419]

Pinaud R, Osorio C, Alzate O, Jarvis ED. Profiling of experience-regulated proteins in the songbird auditory forebrain using quantitative proteomics. Eur J Neurosci. 2008; 27:1409–1422. [PubMed: 18364021]

Popper P, Ishiyama A, Lopez I, Wackym PA. Calcitonin gene-related Peptide and choline acetyltransferase colocalization in the human vestibular periphery. Audiol Neurootol. 2002; 7:298–302. [PubMed: 12232499]

Pujol R, Pickett SB, Nguyen TB, Stone JS. Large basolateral processes on type II hair cells are novel processing units in mammalian vestibular organs. J Comp Neurol. 2014; 522:3141–3159. [PubMed: 24825750]

Ramakrishnan NA, Drescher MJ, Sheikhali SA, Khan KM, Hatfield JS, Dickson MJ, Drescher DG. Molecular identification of an N-type Ca2+ channel in saccular hair cells. Neuroscience. 2006; 139(4):1417–34. [PubMed: 16581196]

Roux I, Wersinger E, McIntosh JM, Fuchs PA, Glowatzki E. Onset of cholinergic efferent synaptic function in sensory hair cells of the rat cochlea. J Neurosci. 2011; 31:15092–15101. [PubMed: 22016543]

Rosenblatt MI, Dickerson IM. Endoproteolysis at tetrabasic amino acid sites in procalcitonin gene-related peptide by pituitary cell lines. Peptides. 1997; 18:567–576. [PubMed: 9210177]

Rossi ML, Prigioni I, Valli P, Casella C. Activation of the efferent system in the isolated frog labyrinth: effects on the afferent EPSPs and spike discharge recorded from single fibres of the posterior nerve. Brain Res. 1980; 185:125–137. [PubMed: 6965463]

Schrott-Fisher A, Egg G, Kong WJ, Renard N, Eybalin M. Immunocytochemical detection of choline acetyltransferase in the human organ of Corti. Hearing Res. 1994; 78(2):149–57.

Safieddine S, Wenthold RJ. SNARE complex at the ribbon synapses of cochlear hair cells: analysis of synaptic vesicle- and synaptic membrane-associated proteins. Eur J Neurosci. 1999; 11:803–812. [PubMed: 10103074]

Sans A, Highstein SM. New ultrastructural features in the vestibular labyrinth of the toadfish, Opsanus tau. Brain Res. 1984; 308:191–195. [PubMed: 6332657]

Simmons DD, Tong B, Schrader AD, Hornak AJ. Oncomodulin identifies different hair cell types in the mammalian inner ear. J Comp Neurol. 2010; 518:3785–3802. [PubMed: 20653034]

Sliwinska-Kowalska M, Parakkal M, Schneider ME, Fex J. CGRP-like immunoreactivity in the guinea pig organ of Corti: a light and electron microscopy study. Hear Res. 1989; 42:83–95. [PubMed: 2584160]

Soni LE, Warren CM, Bucci C, Orten DJ, Hasson T. The unconventional myosin-VIIa associates with lysosomes. Cell Motil Cytoskeleton. 2005; 62:13–26. [PubMed: 16001398]

Sugai T, Sugitani M, Ooyama H. Effects of activation of the divergent efferent fibers on the spontaneous activity of vestibular afferent fibers in the toad. Jpn J Physiol. 1991; 41:217–232. [PubMed: 1942662]

Tanaka M, Takeda N, Senba E, Tohyama M, Kubo T, Matsunaga T. Localization, origin and fine structure of calcitonin gene-related peptide-containing fibers in the vestibular end-organs of the rat. Brain Res. 1989; 504:31–35. [PubMed: 2598015]

Tremere LA, Jeong JK, Pinaud R. Estradiol shapes auditory processing in the adult brain by regulating inhibitory transmission and plasticity-associated gene expression. J Neurosci. 2009; 29:5949–5463. [PubMed: 19420261]

Velho TA, Mello CV. Synapsins are late activity-induced genes regulated by birdsong. J Neurosci. 2008; 28:11871–11882. [PubMed: 19005052]

Wackym PA, Popper P, Ward PH, Micevych PE. Cell and molecular anatomy of nicotinic acetylcholine receptor subunits and calcitonin gene-related peptide in the rat vestibular system. Otolaryngol Head Neck Surg. 1991; 105:493–510. [PubMed: 1762788]

Wibowo E, Brockhausen J, Koppl C. Efferent innervation to the auditory basilar papilla of scincid lizards. J Comp Neurol. 2009; 516:74–85. [PubMed: 19565665]

Zheng JL, Gao WQ. Analysis of rat vestibular hair cell development and regeneration using calretinin as an early marker. J Neurosci. 1997; 17:8270–8282. [PubMed: 9334402]

Zidanic M. Cholinergic innervation of the chick basilar papilla. J Comp Neurol. 2002; 445:159–175. [PubMed: 11891660]

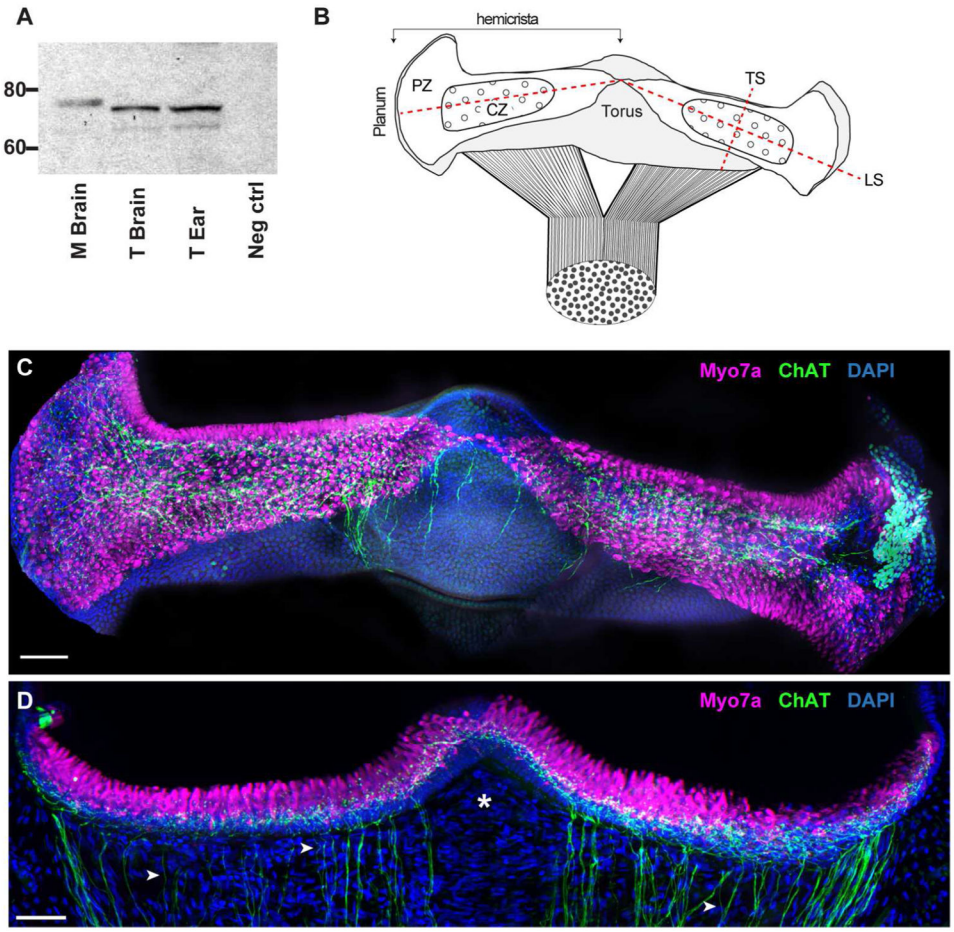

Figure 1.

The expression of ChAT in turtle canal cristae. **A**. Specificity of the ChAT antibody (AB144P) was confirmed via western blotting of turtle and mouse tissues. Both tissues showed ChAT immunoreactivity within the appropriate range of molecular weights. Lanes (left to right): 1, Mouse brain; 2, Turtle brain; 3, Turtle ear; 4, negative control. **B**. Diagram of the intact turtle posterior crista modeled after the immunostained whole organ micrograph shown in panel C. The canal nerve bifurcates to innervate two triangular-shaped hemicrista that extend from the planum to the nonsensory torus. Each hemicrista consists of a central zone (CZ) and peripheral zone (PZ). Dashed lines indicate planes of sectioning used in this study (LS – longitudinal section; TS – transverse section). **C**. Apotome image projection of a whole crista preparation of the turtle posterior crista where cholinergic fibers (green) and hair cells (magenta) were labeled with antibodies to ChAT and Myo7A, respectively. Nuclear staining with DAPI is shown in blue. **D**. Confocal image projection of a longitudinal section of the turtle posterior crista stained for ChAT (green) and Myo7A (magenta). Intense DAPI staining (blue) below hair cells demarcates supporting cell layer. Arrowheads identify single ChAT-positive fibers and asterisk demarcates stromal region devoid of efferent fibers. Scale bars = 50 μm.

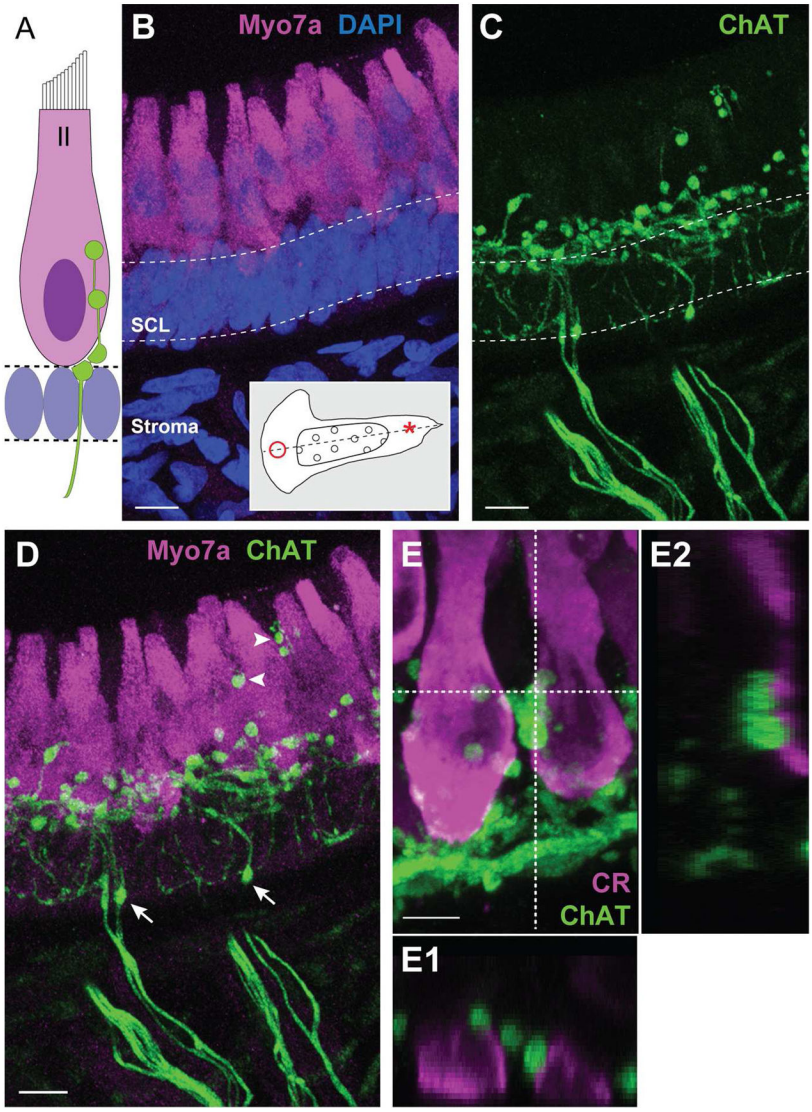

Figure 2.

ChAT-positive fibers give rise to numerous spherical varicosities in the hair cell layer. **A**. Illustration depicting common locations of efferent terminals on type II hair cells. Supporting cell nuclei fill the space beneath the hair cell layer. **B**. Confocal image projection of a longitudinal section of the turtle crista where type II hair cells near the torus (asterisk, inset) were stained with antibodies to Myo7A (magenta). Dense DAPI staining (blue) emphasizes the supporting cell layer (SCL, dashed lines). **C**. Efferent fibers and associated varicosities were labeled with antibodies to ChAT (green) in the same section shown in panel B. **D**. Combined image details the arrangement of ChAT-positive varicosities along type II hair cells. Arrows indicate ChAT-positive varicosities located well below the hair cell layer. Arrowheads identify more apical ChAT-positive varicosities. **E**. Confocal image projection of a longitudinal section of the turtle crista showing type II hair cells near the planum stained with antibodies to calretinin (magenta). ChAT-positive varicosities (green) populate the basal pole. **E1**, **E2**. Orthogonal views, generated along the dashed lines,

indicate the relative position of ChAT-positive varicosities within the Z-plane. Scale bar = 10 μm in **B**–**D**, 5 μm in **E**.

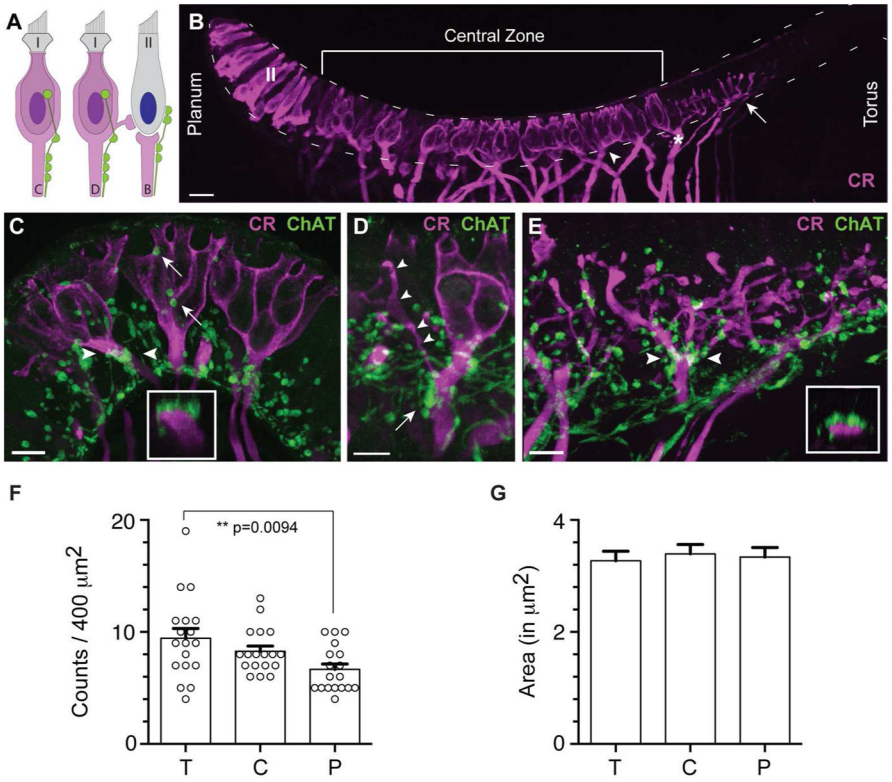

Figure 3.

ChAT-positive varicosities are found abutting afferent fibers in the turtle crista. **A**. Illustration depicting locations of efferent terminals on calyx (C), dimorphic (D), and bouton (B) afferents. Efferent terminals on a type II hair cell are also shown. **B**. Confocal image projection of a longitudinal section of a turtle hemicrista stained with antibodies to calretinin (magenta). Anti-calretinin labeled calyx afferents (arrowhead), dimorphic afferents (asterisk), bouton afferents near the torus (arrow), and type II hair cells near the planum (II). Dashed lines border the hair cell layer from the planum to the torus. **C**. Confocal image projection of a transverse section through the central zone of a turtle hemicrista showing ChAT-positive varicosities (green) clustered along the axonal stalk of calretinin-positive calyx afferents (magenta). Inset: Orthogonal view generated for the calyx afferent bracketed by arrowheads demonstrating the proximity of ChAT-positive varicosities to the parent fiber. ChAT-positive varicosities are also identified along segments of the calyceal expansion (arrows). **D**. ChAT-positive varicosities (green) are similarly distributed on the axonal stalk (arrow) of a calretinin-positive dimorphic afferent (magenta). Bouton offshoot of dimorphic afferent indicated by arrowheads. **E**. A confocal image projection of bouton afferents near the torus was taken from a longitudinal section of the turtle crista stained with antibodies to calretinin (magenta) and ChAT (green). Inset: Orthogonal view (between arrowheads) indicates the proximity of varicosities to the bouton afferent fiber just prior to a branch point. Scale bar = 20 µm in all panels. **F**. ChAT-positive varicosities were counted across the zones of the turtle crista (T=torus, C=central, P=planum). Average counts from torus and planum regions were significantly different ($p<0.01$) while neither torus nor planum were significantly different from the central zone. Circles indicate mean counts for

each 20μm × 20μm area sampled (n=18). **G**. Mean ChAT varicosity areas were also calculated and found to be similar across all three zones. Error bars = SEM.

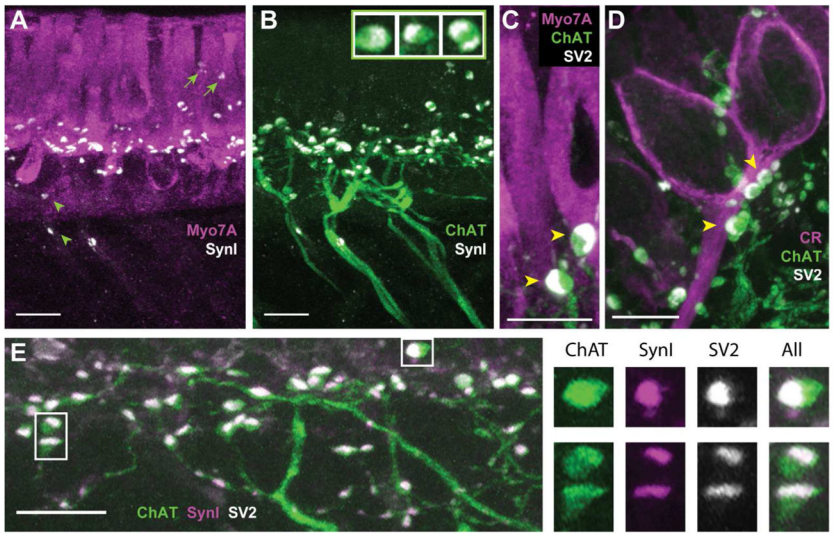

Figure 4.

The synaptic vesicle proteins synapsin I and SV2 colocalize with ChAT in efferent varicosities of the turtle crista. **A**, **B**. Confocal image projection was generated from a longitudinal section of the turtle crista stained with antibodies to Myo7A (magenta), synapsin I (SynI, white), and ChAT (green). **A**. Antibodies to SynI labeled numerous puncta along the basal end of type II hair cells near the torus. A few SynI-positive puncta were also located the above hair cell nuclei (arrows) and below the hair cell layer (arrowheads). **B**. Most of the puncta stained with antibodies to SynI appeared restricted to ChAT-positive varicosities. Inset: Zoomed images showing colocalization and distribution of ChAT (green) and synI (white) within three efferent varicosities. **C**, **D**. Confocal image projections were generated from transverse sections of the turtle crista previously stained with antibodies to Myo7A (magenta in panel C) or CR (magenta in panel D) with ChAT (green), and SV2 (white). Several efferent varicosities cluster along the base of a type II hair cell near the torus (panel C) and calyx afferent from the central zone (panel D). **E**. A confocal image projection of efferent fibers and varicosities near the torus taken from a longitudinal section of a turtle crista stained for ChAT (green), SynI, (magenta), and SV2 (white). Right panels show zoomed images of three efferent varicosities (boxes, panel D) showing the colocalization and distribution of ChAT, synI, and SV2. Scale bar = 10 μm in all panels.

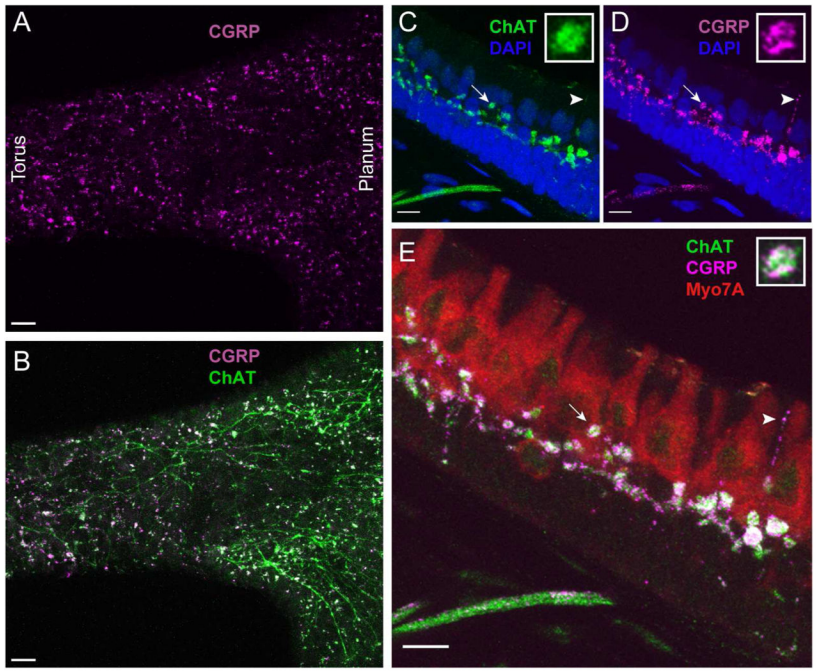

Figure 5.

Efferent varicosities in turtle cristae also express the neuropeptide CGRP. **A**, **B**. Apotome image projection of a whole organ preparation of a turtle posterior crista stained with antibodies to CGRP (magenta) and ChAT (green). **C**–**E**. A confocal image projection taken near the torus of a longitudinal section of a turtle hemicrista stained with antibodies for CGRP (magenta), ChAT (green), and Myo7A (red). Insets: Zoomed image of an efferent varicosity (arrow) showing colocalization and distribution of ChAT and CGRP. Arrowhead points to efferent tendril-like extension into the hair cell layer. Scale bar = 20 μm in **A**, **B** and 10 μm in panels **C**–**E**.

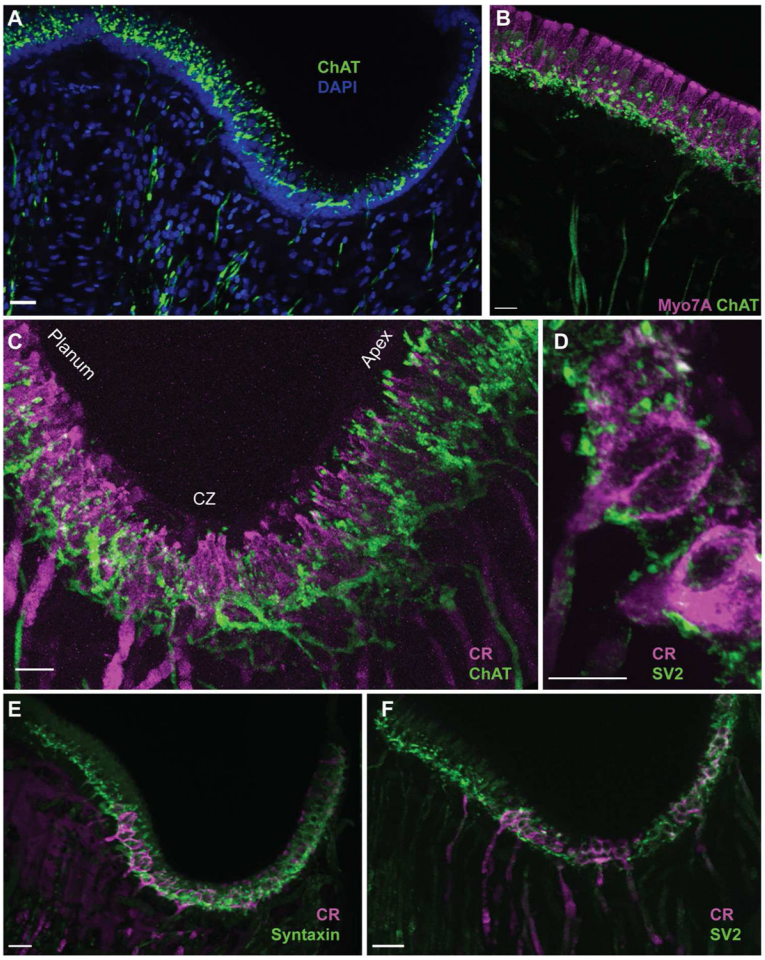

Figure 6.

ChAT is a marker of vestibular efferents in bird cristae. For all panels, confocal image projections were taken from longitudinal sections of Zebra Finch cristae. **A**. Antibodies to ChAT (green) labeled efferent fibers in the stroma and associated varicosities across the crista. DAPI staining (blue) demarcated the supporting cell layer. **B**. Type II hair cells near the apex were stained with antibodies to Myo7A (magenta) while efferent fibers and varicosities along the basal half of the hair cell layer were stained with antibodies to ChAT (green). **C**. Calyx-bearing afferents in the central zone of the bird crista stained with antibodies against calretinin (magenta). ChAT-positive varicosities (green) densely populated the central zone. **D**. Numerous puncta labeled with antibodies to SV2 (green) appose calyx-bearing afferents stained for calretinin (magenta). **E**, **F**. Confocal image projections of bird hemicrista stained with antibodies to calretinin (magenta) and syntaxin (green, panel E) or SV2 (green, panel F). Scale bar = 10 μm.

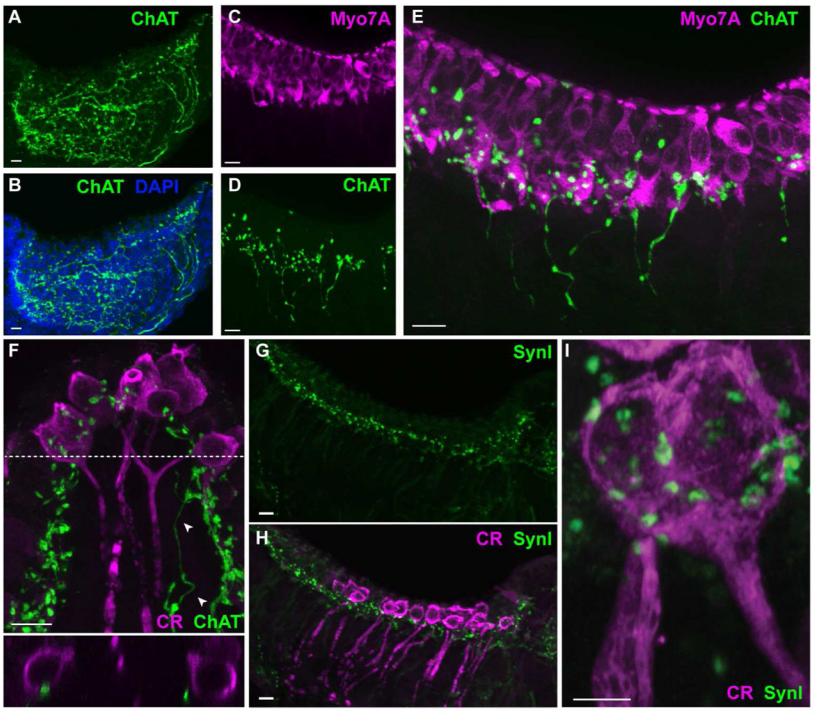

Figure 7.

ChAT is a marker of vestibular efferents in mouse cristae. Confocal image projections were generated from either longitudinal (panels A–E, G–I) or transverse (panel F) sections of the mouse crista. **A**, **B**. Antibodies to ChAT (green) labeled efferent fibers and varicosities across the crista. DAPI staining (blue) defines the tissue boundaries. **C**. Hair cells in the mouse crista were stained with antibodies to Myo7A (magenta). **D**. Efferent fibers and associated varicosities were labeled with antibodies to ChAT (green) in the same section shown in panel C. **E**. Combined image from panels C and D shows ChAT-positive varicosities scattered along the hair cell layer. **F**. Calyx-bearing afferents in the central zone of the mouse crista stained with antibodies against calretinin (magenta). ChAT-positive varicosities (green) are distributed across the neuroepithelium with several located in close apposition to calyx endings. A ChAT-positive fiber can be seen on the right (arrowheads). Bottom panel: Orthogonal view along dashed line indicates the proximity of varicosities to the outer face of two calyx endings. **G**, **H**. Confocal image projections of mouse hemicrista stained with antibodies to SynI (green) and calretinin (magenta), respectively. **I**. An enlarged image of a calretinin-positive calyx (magenta) shows the location of several SynI-positive puncta. Scale bar = 10 μm except Panel I which is 5 μm.

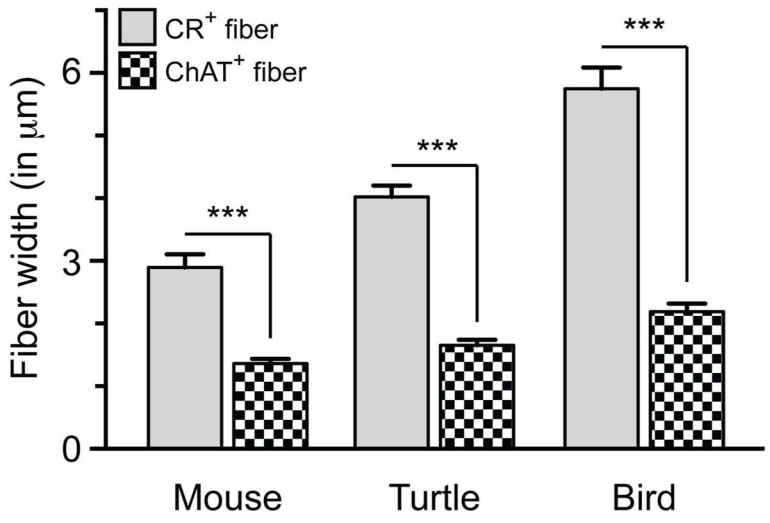

Figure 8.

Fiber diameter measurements of ChAT+ efferent fibers vs CR+ calyx fibers in mouse, turtle and bird cristae. Note that for each species, CR+ calyx fibers were significantly larger in diameter than ChAT+ fibers for the same species (two-way ANOVA with Bonferonni multiple planned comparisons, ***$p<0.0001$). Interestingly, CR+ fiber diameters were also significantly different between species ($p\leq0.01$) while ChAT+ fibers were only different in size between bird and mouse ($p<0.05$). Bars represent mean diameters ± SEM ($n = 10$).

Table 1

Antibody (Dilution)	Immunogen	Catalog#/Manufacturer/ Lot#	Specificity Controls	
			Validation	Staining Pattern
Calretinin (1:1000)	Rat calretinin	Millipore AB1550 lot LV148604 Polyclonal (goat), RRID: AB_90764	Immunoblot: Manufacturer, Hackney et al., 2003;	Type II hair cells and afferents as reported (Desai et al., 2005; Pujol et al. 2014)
Calretinin (1:1000)	Rat calretinin	Chemicon AB5054 lot LV1552190 Polyclonal (rabbit), RRID: AB_2068506	Immunoblot: Manufacturer, Hackney et al., 2003; Liu and Davis, 2014.	Type II hair cells and afferents as reported (Desai et al., 2005; Pujol et. al 2014)
CGRP (1:500)	amidated carboxyl 7aa of rat αCGRP	Mu33; a kind gift from Ian Dickerson Polyclonal (rabbit)	Immunprecipitation: Rosenblatt and Dickerson, 1997	Efferent fibers and varicosities as reported (Demêmes et al., 2001; Luebke et al., 2014)
CGRP (1:500)	Mature rat full length αCGRP	JH84; A kind gift from Ian Dickerson Polyclonal (rabbit)	Immunprecipitation: Rosenblatt and Dickerson, 1997	Efferent fibers and varicosities as reported (Demêmes et al., 2001; Luebke et al., 2014)
Choline Acetyltransferase (1:100)	Human placental enzyme	Chemicon AB144P lot JC1618187 Polyclonal (goat) RRID:AB_2079751	Immunoblot: Lee et al., 2007); Wibowo et al. 2009.	Efferent fibers and varicosities as reported (Ohno et al., 1993; Kong et al., 1994)
Choline Acetyltransferase (1:500)	Chick brain	A kind gift from Dr. Epstein Polyclonal (rabbit) RRID: AB_2314177	Immunoblot: Johnson and Epstein, 1986	Efferent fibers and varicosities as reported (Ohno et al., 1993; Kong et al. 1994; Zidanic 2002)
Myosin VIIA 10 μg/ml	aa880-1077 from the tail region of human Myo7A	Proteus #25-6790, Polyclonal (rabbit) RRID:AB_10015251	Immunoblot: Hasson et al., 1995	Type I and II hair cells as reported (Hasson et al. 1997; Duncan et al., 2006)
Myosin VIIA* (1:100)	aa927-1203 from human Myo7A	DSHB #138-1, Monoclonal (mouse) RRID:AB_2282417	Immunoblot: Soni et al., 2005	Type I and II hair cells as reported (Hasson et al. 1997; Duncan et al., 2006)
Synapsin I (1:500–1000)	Bovine Synapsin I (mixture of Ia and Ib)	Chemicon AB1543 lot LV1463637 Polyclonal (rabbit), RRID:AB_2200400	Immunoblot: Kopeikina et al., 2013.	Punctated labeling of efferent varicosities (Favre et al., 1986; Holstein et al., 2005)
SV2** 1:200–10,000	Synaptic vesicle (Ommata electric organ)	DSHB SV2 conc. Ascites, Monoclonal (mouse), RRID:AB_2315408	Immunoblot: Buckley and Kelly 1995; Wibowo et al. 2009	Punctated labeling of efferent varicosities (Layton et al., 2005; Wibowo et al., 2009).
Syntaxin (1:1000)	Synaptosomal plasma membrane fraction from adult rat hippocampus	Sigma #S0664 Clone HPC-1 lot 019K4834, Monoclonal (mouse) RRID:AB_477483	Immunoblot: Barnstable et al. 1985; Inoue et al., 1992; see also manufacturer data sheet	Punctated labeling of efferent varicosities (Hennig and Cotanche, 1998)

* Generated by Dana Jo Orten

** Developed by K. Buckley. Both were obtained from the Developmental Studies Hybridoma Bank developed under the auspices